Sterically shielded primary anilides of the alkaline-earth metals of the type $(thf)_nAe(NH\text{-}Ar^*)_2$ (Ae = Mg, Ca, Sr, and Ba; Ar* = bulky aryl)

Philipp Schüler,[a] Sven Krieck,[a] Helmar Görls,[a] Phil Liebing,[a] and Matthias Westerhausen*[,a]

[a] *Institute of Inorganic and Analytical Chemistry, Friedrich Schiller University Jena Humboldtstraße 8, D-07743 Jena, Germany e-mail: m.we@uni-jena.de*

Content

1 Analytical data

1.1 $[(thf)_2Mg(NH\text{-}C_6H_2(Ph)_3)_2]$ **1b**

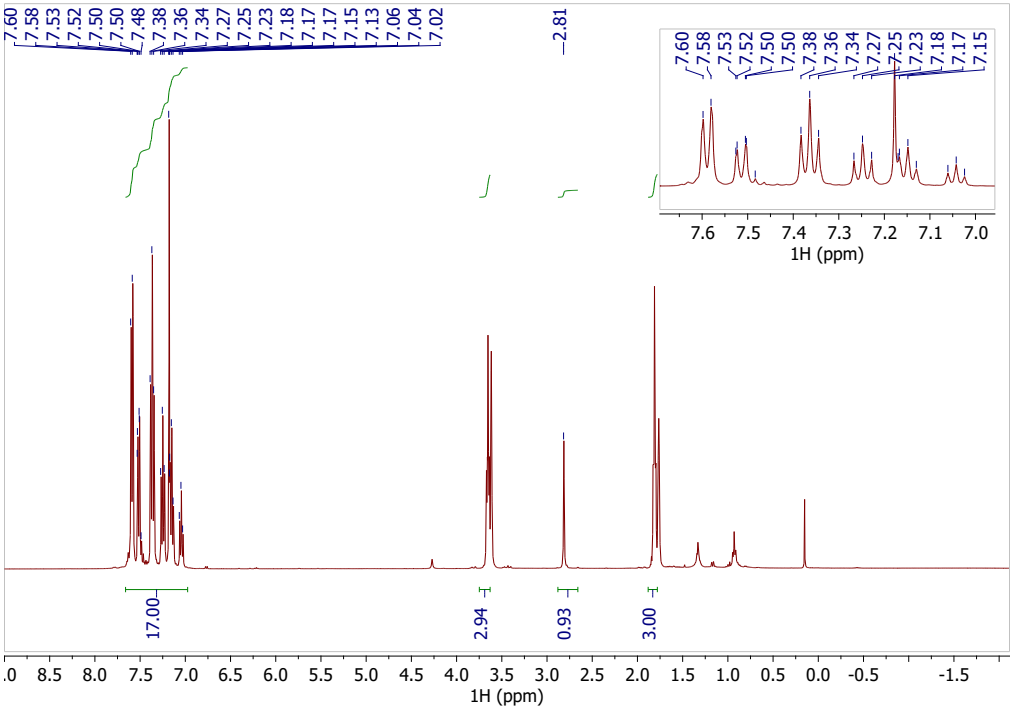

Figure S 1: ^{1}H-NMR-Spectrum (400 MHz, [D_8]THF, 297 K) of $[(thf)_2Mg(HN\text{-}(Ph)_3C_6H_2)_2]$ **1b**.

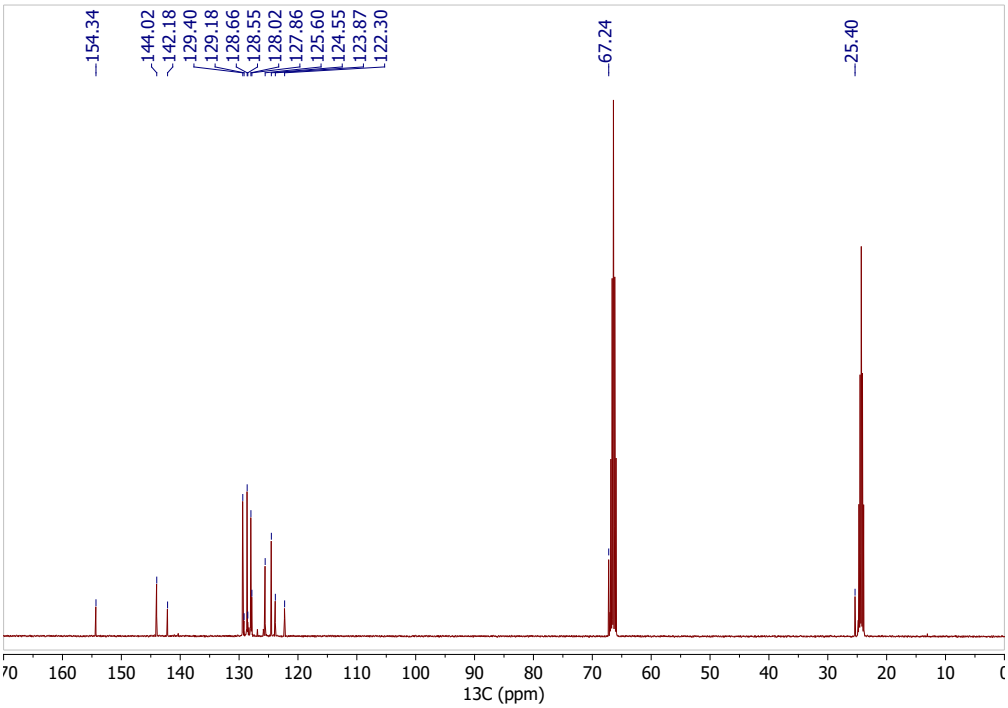

Figure S 2: $^{13}C\{^{1}H\}$-NMR -Spectrum (101 MHz, [D_8]THF, 297 K)of $[(thf)_2Mg(HN\text{-}(Ph)_3C_6H_2)_2$ **1b**.

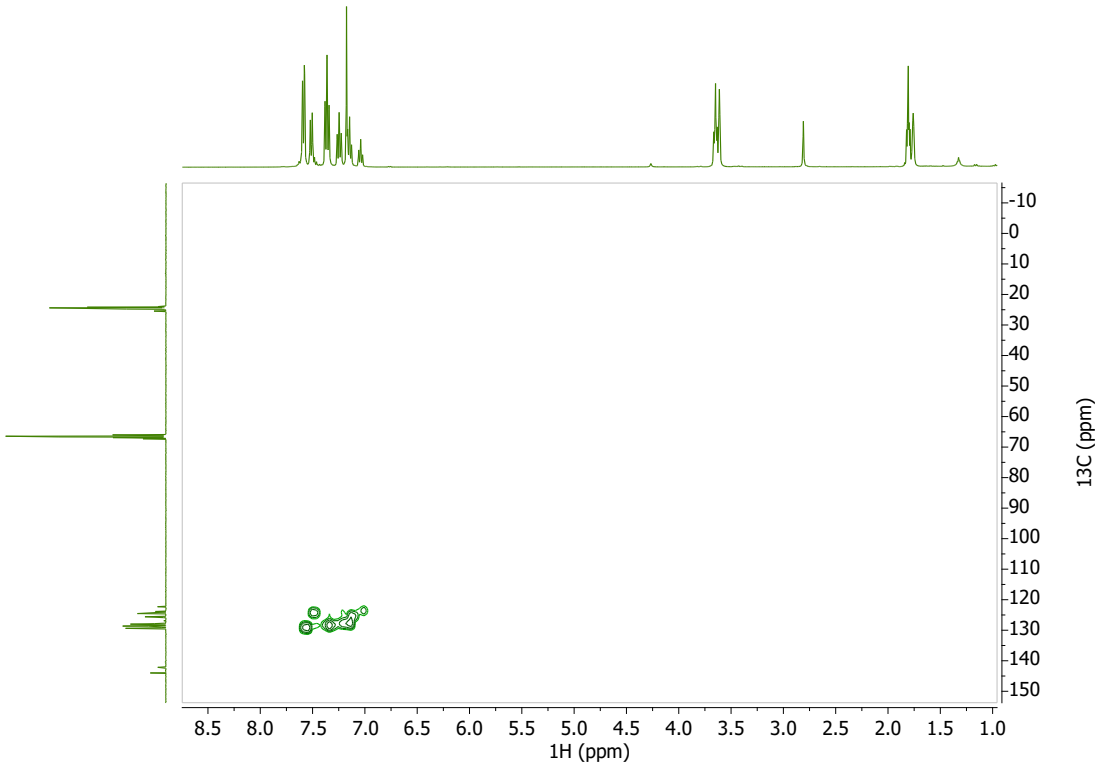

Figure S 3: HSQC-NMR-Spectrum (400 MHz, $[D_8]$THF, 297 K) of $[(thf)_2Mg(HN\text{-}(Ph)_3C_6H_2)_2]$ **1b**.

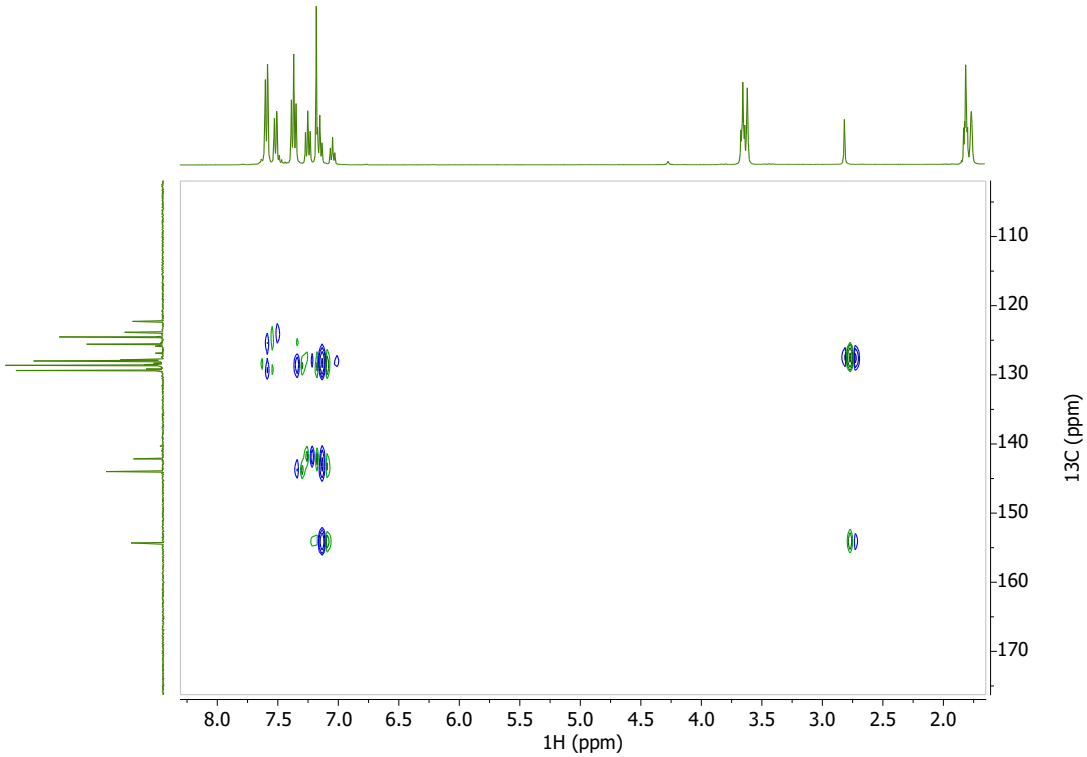

Figure S 4: HMBC-NMR-Spectrum (400 MHz, $[D_8]$THF, 297 K) of $[(thf)_2Mg(HN\text{-}(Ph)_3C_6H_2)_2]$ **1b**.

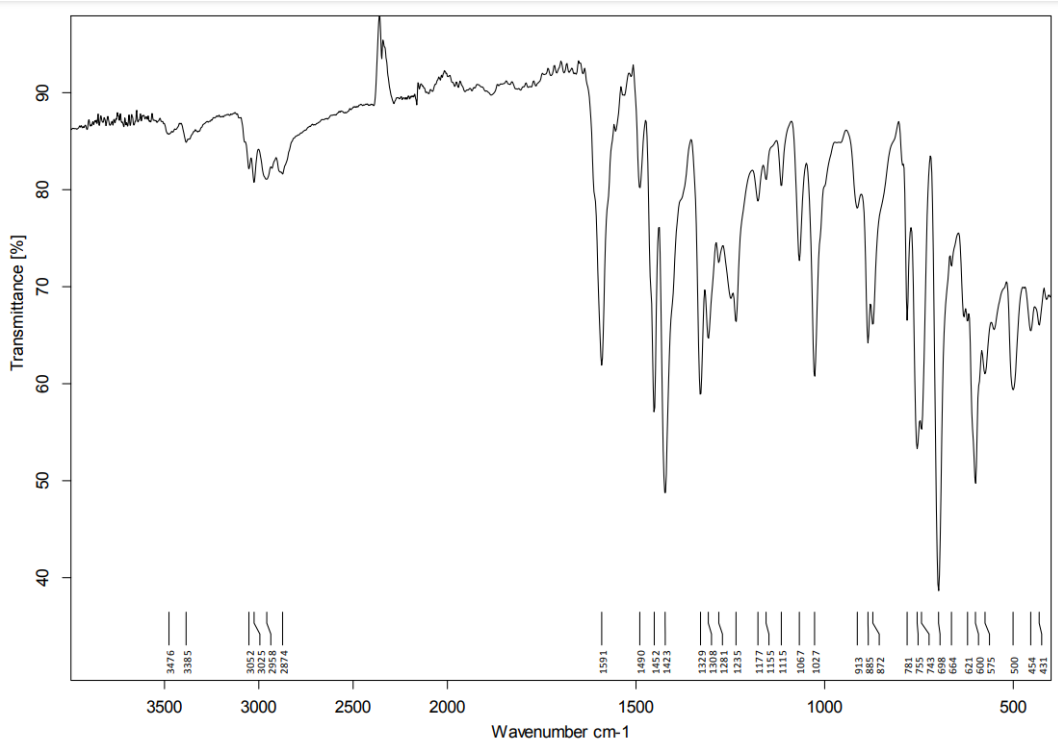

Figure S 5: IR spectrum (ATR) of $[(thf)_2Mg(HN\text{-}(Ph)_3C_6H_2)_2]$ **1b**.

1.2 $[(thf)_2Ca(NH\text{-}C_6H_2(Ph)_3)_2]$ **1c**

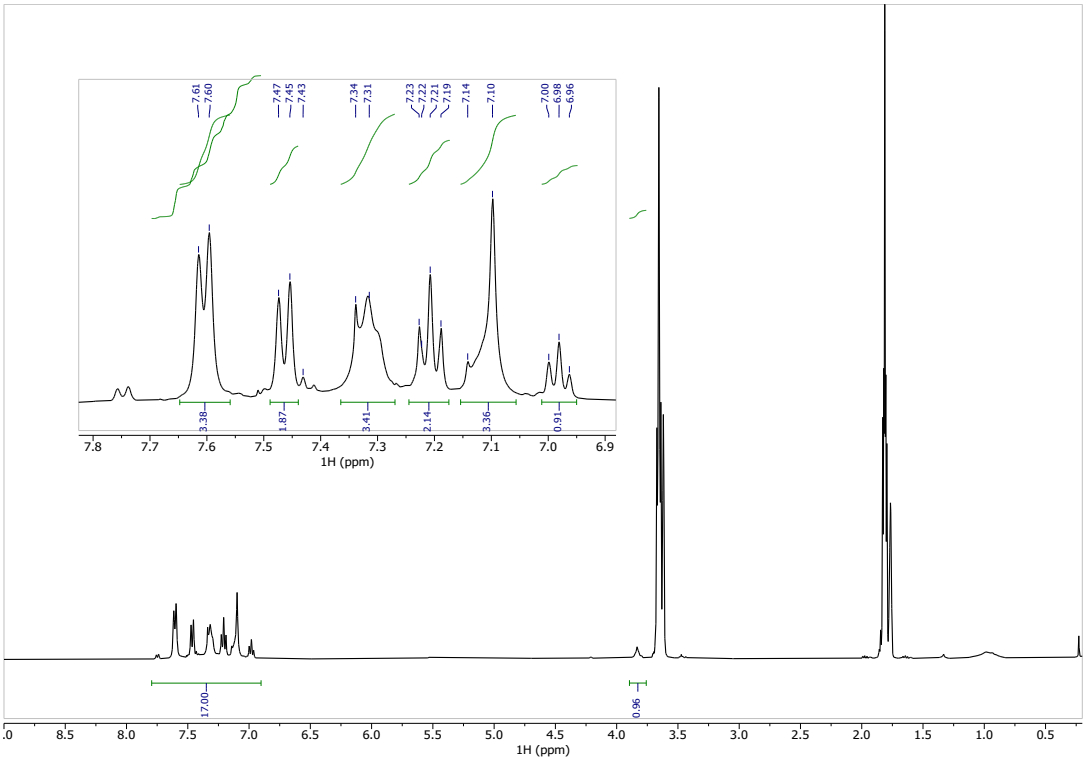

Figure S 6: ^{1}H-NMR-Spectrum (400 MHz, $[D_8]$THF, 297 K) of $[(thf)_2Ca(NHC_6H_2(Ph)_3)_2]$ **1c**.

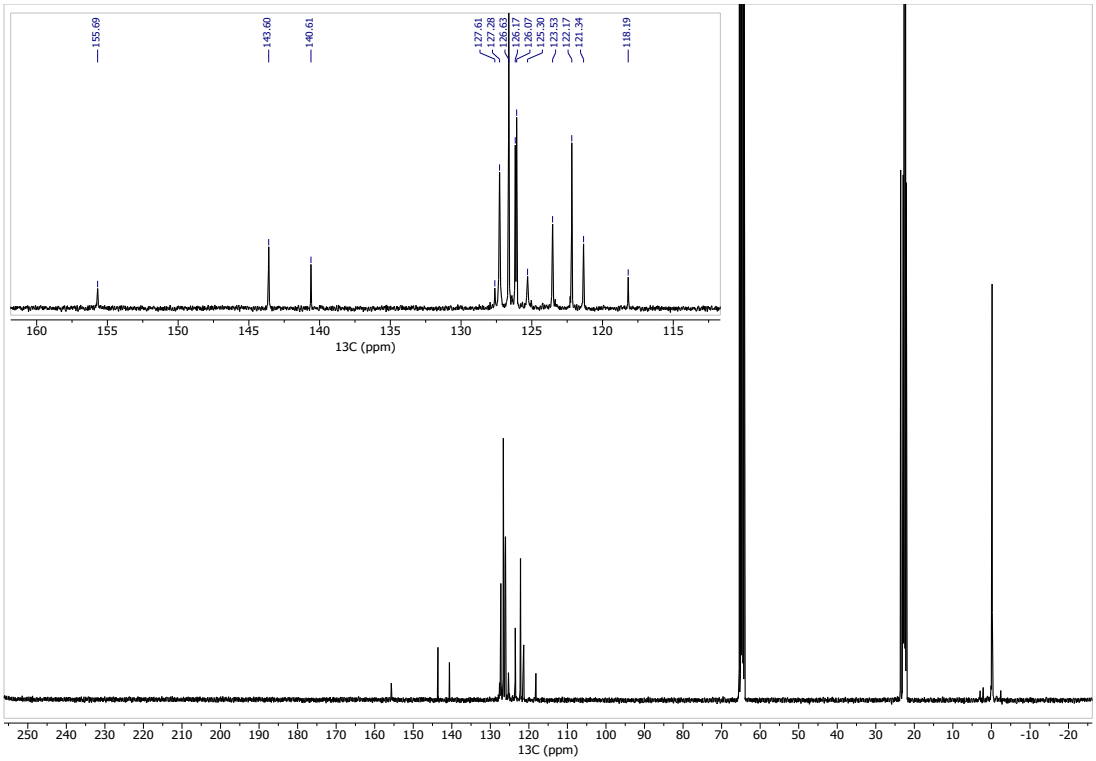

Figure S 7: $^{13}C\{^{1}H\}$-NMR-Spectrum (101 MHz, $[D_8]$THF, 297 K) of $[(thf)_2Ca(NHC_6H_2(Ph)_3)_2]$ **1c**.

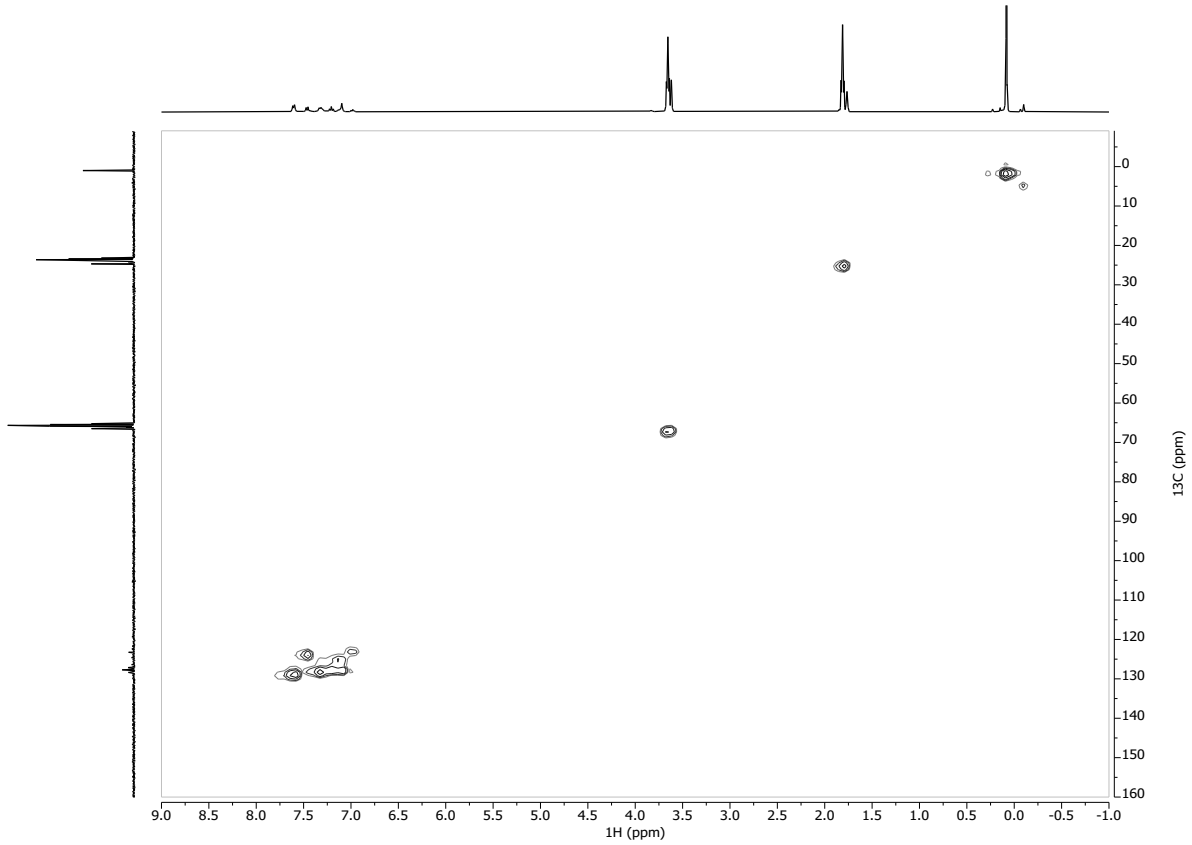

Figure S 8: HSQC-NMR-Spectrum (400 MHz, [D_8]THF, 297 K) of [$(thf)_2Ca(NHC_6H_2(Ph)_3)_2$] **1c**.

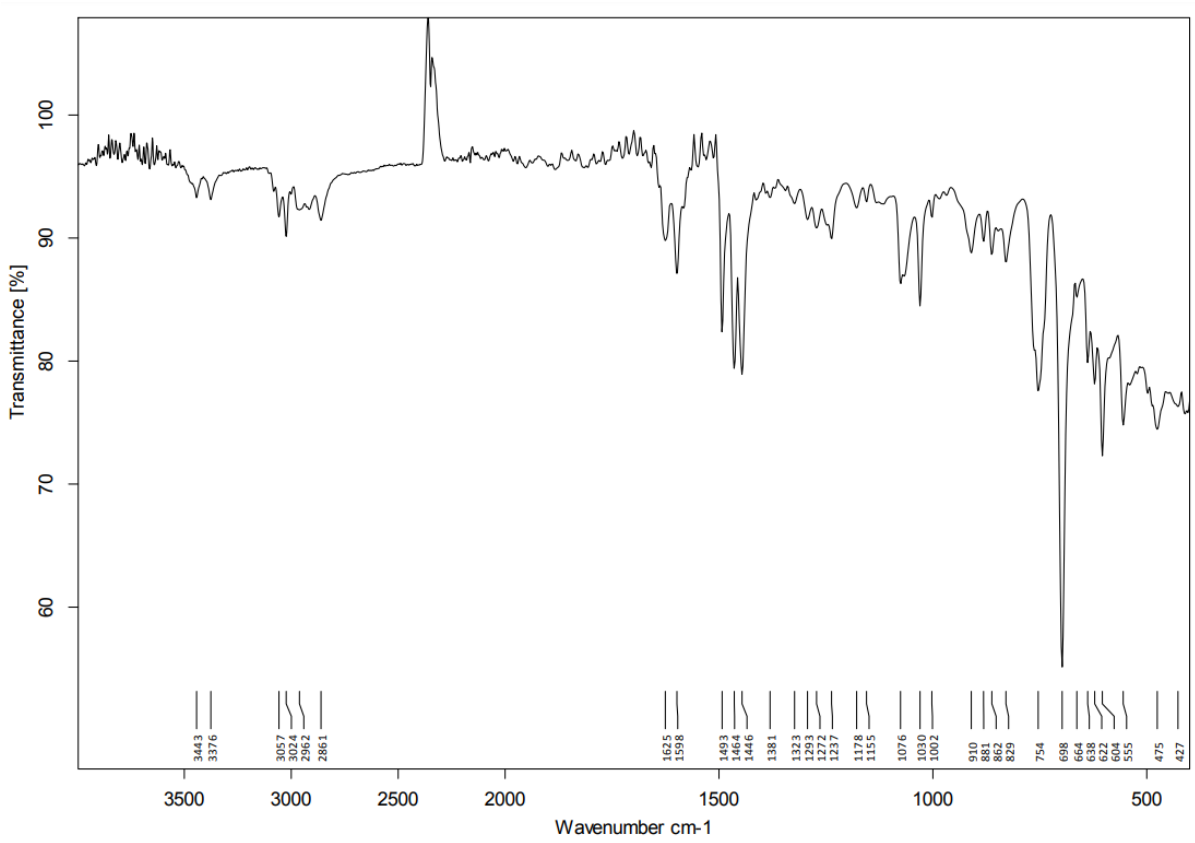

Figure S 9: IR spectrum (ATR) of [$(thf)_2Ca(NHC_6H_2(Ph)_3)_2$] **1c**.

1.3 $[(thf)_3Sr(NH\text{-}C_6H_2(Ph)_3)_2]$ **1d**

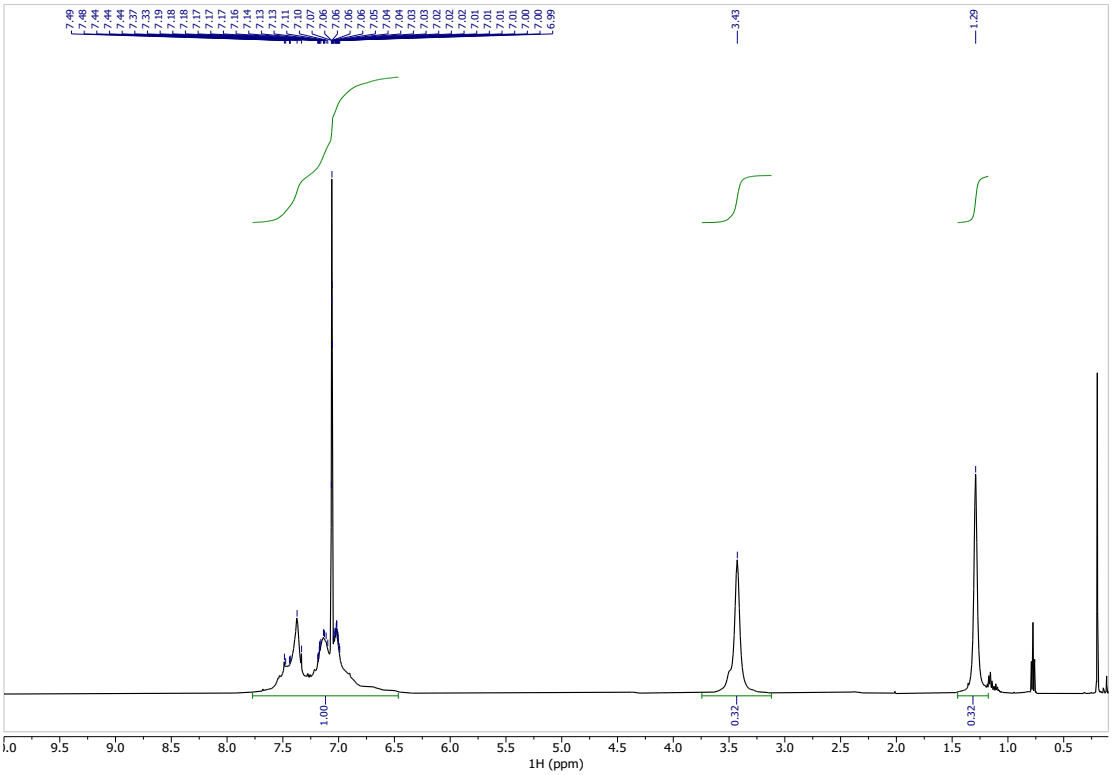

Figure S 10: ^{1}H-NMR-Spectrum (400 MHz, C_6D_6, 297 K) of $[(thf)_3Sr\{NH\text{-}2,4,6\text{-}(Ph)_3\text{-}C_6H_2]$ **1d**.

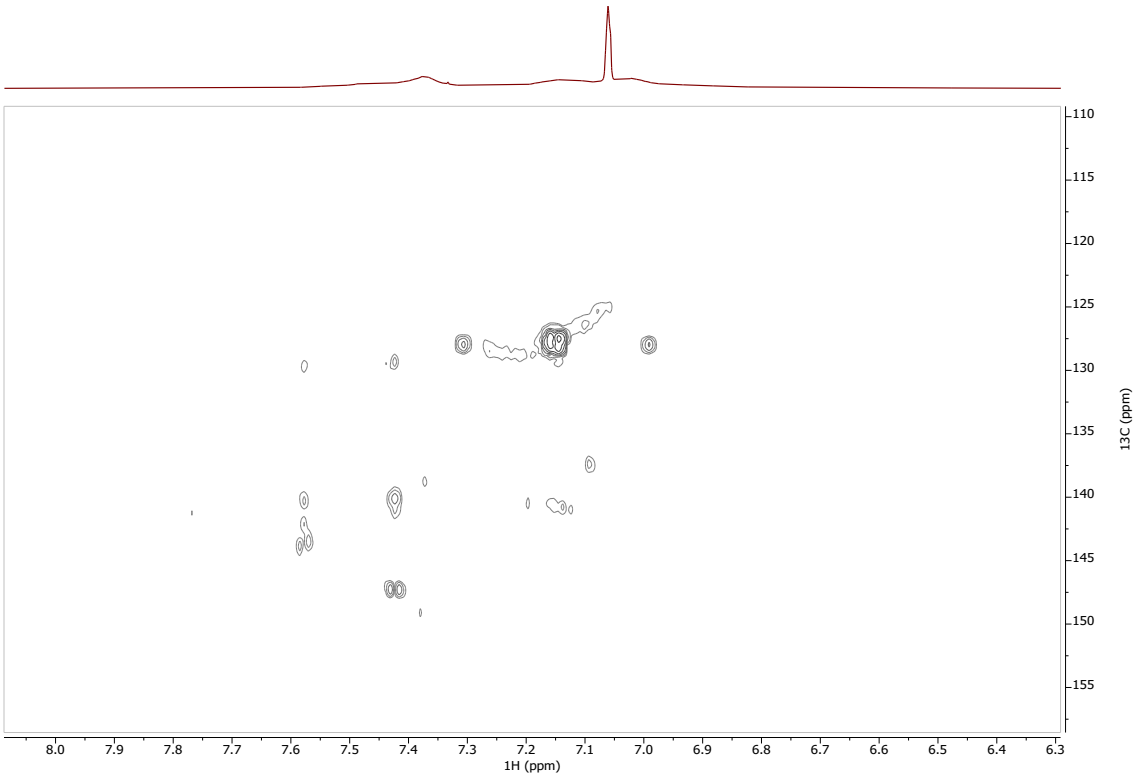

Figure S 11: HMBC -NMR-Spectrum (400 MHz, C_6D_6, 297 K) of $[(thf)_3Sr\{NH\text{-}2,4,6\text{-}(Ph)_3\text{-}C_6H_2]$ **1d**.

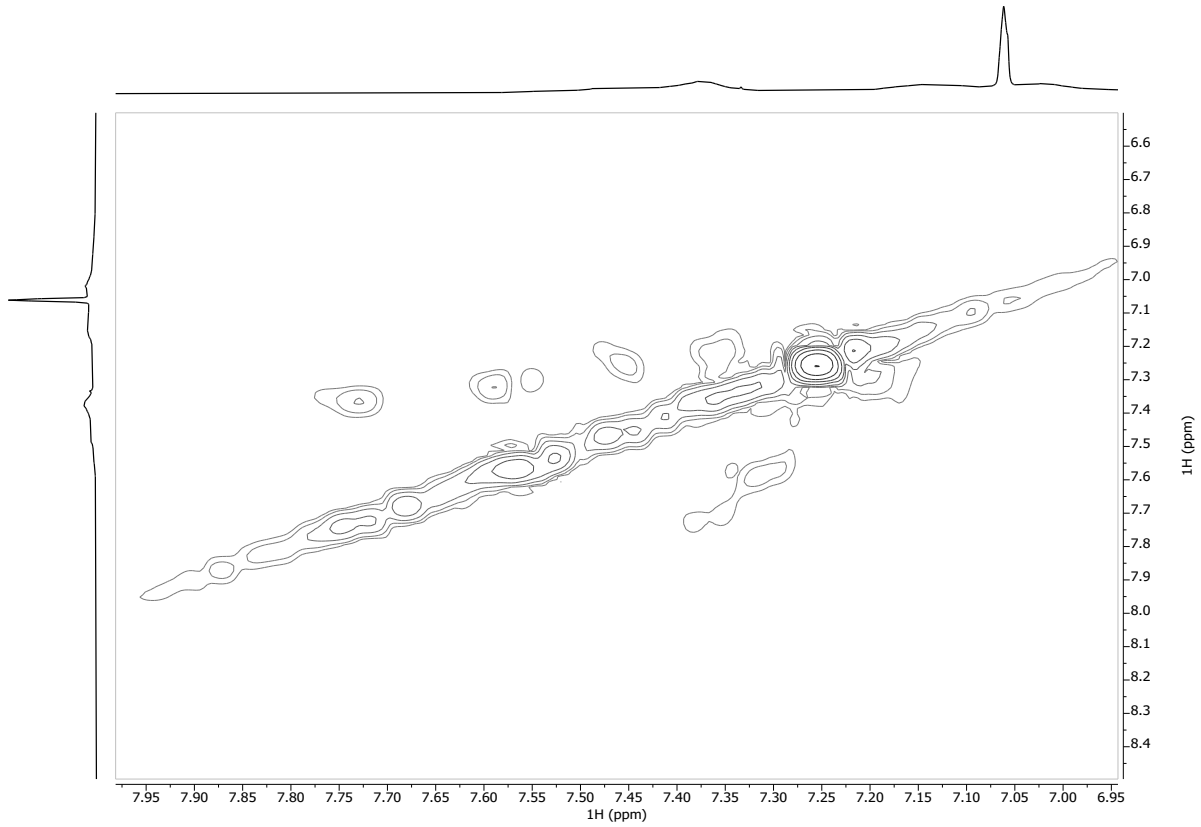

Figure S 12: H,H-COSY-NMR-Spektrum (400 MHz, C_6D_6, 297 K) von$[(thf)_3Sr\{NH\text{-}2,4,6\text{-}(Ph)_3\text{-}C_6H_2]$ **1d**.

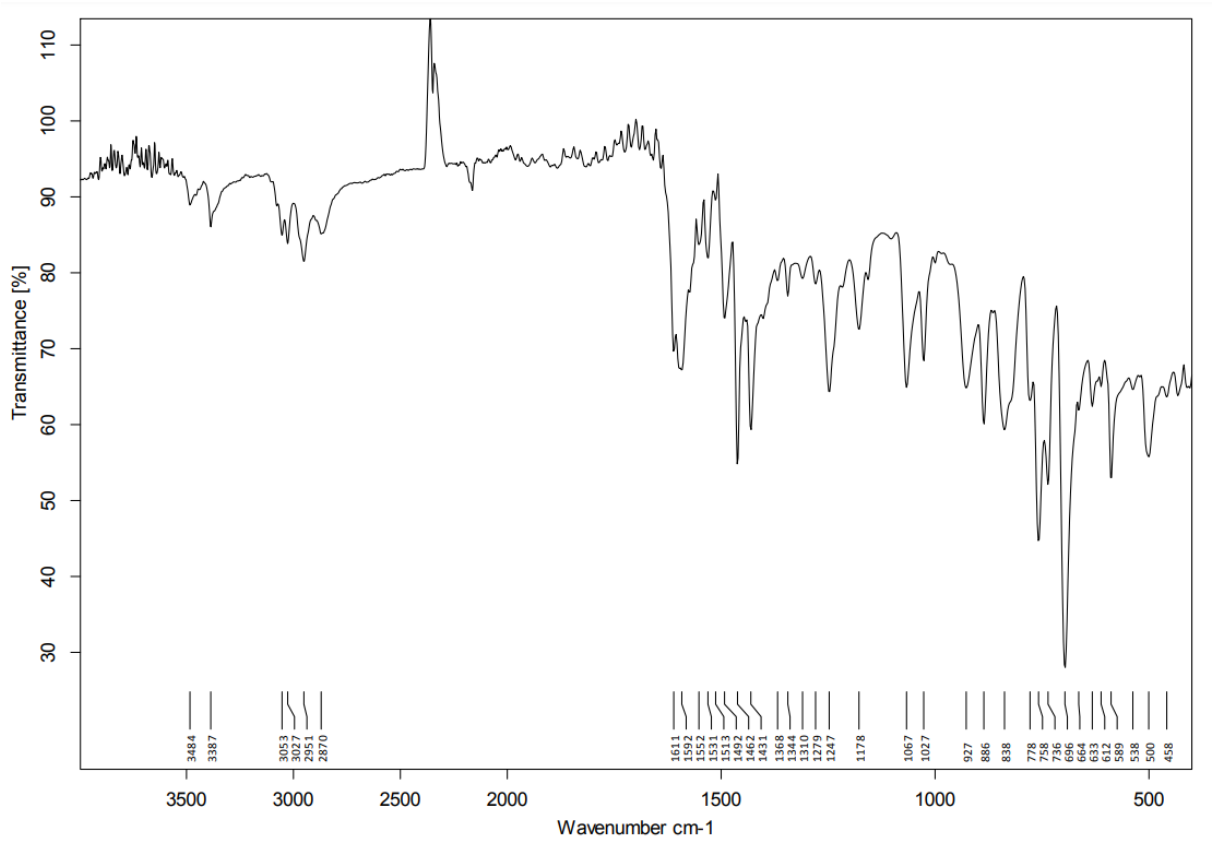

Figure S 13: IR spectrum (ATR) of $[(thf)_3Sr\{NH\text{-}2,4,6\text{-}(Ph)_3\text{-}C_6H_2]$ **1d**.

1.4 $[(thf)_3Ba(NH\text{-}C_6H_2(Ph)_3)_2]$ **1e**

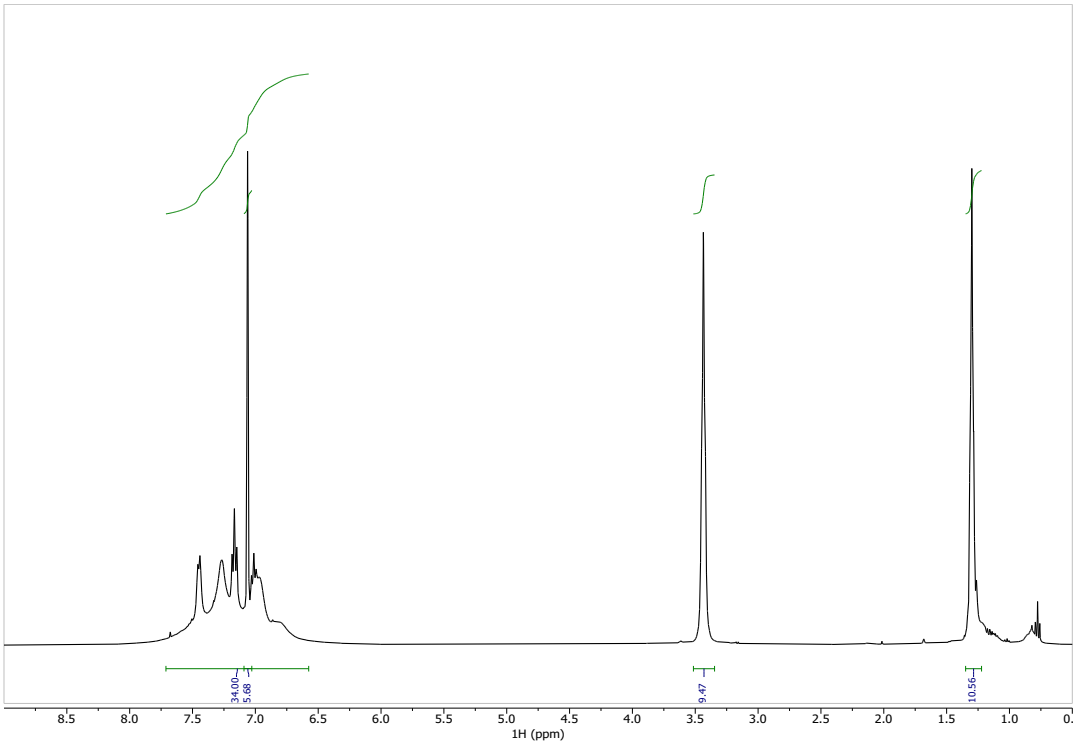

Figure S 14: ^{1}H-NMR-Spectrum (400 MHz, C_6D_6, 297 K) of $[(thf)_3Ba(NH\text{-}C_6H_2(Ph)_3)_2]$ **1e**.

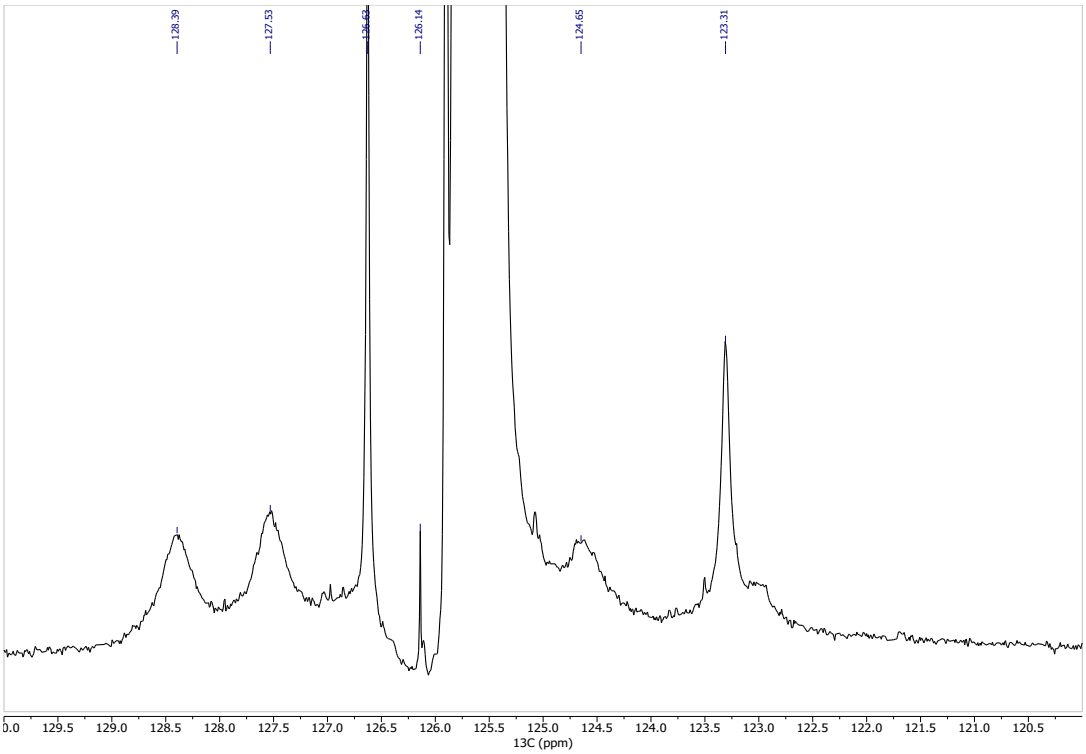

Figure S 15: $^{13}C\{^{1}H\}$-NMR-Spectrum (101 MHz, C_6D_6, 297 K) of $[(thf)_3Ba(NH\text{-}C_6H_2(Ph)_3)_2]$ **1e**.

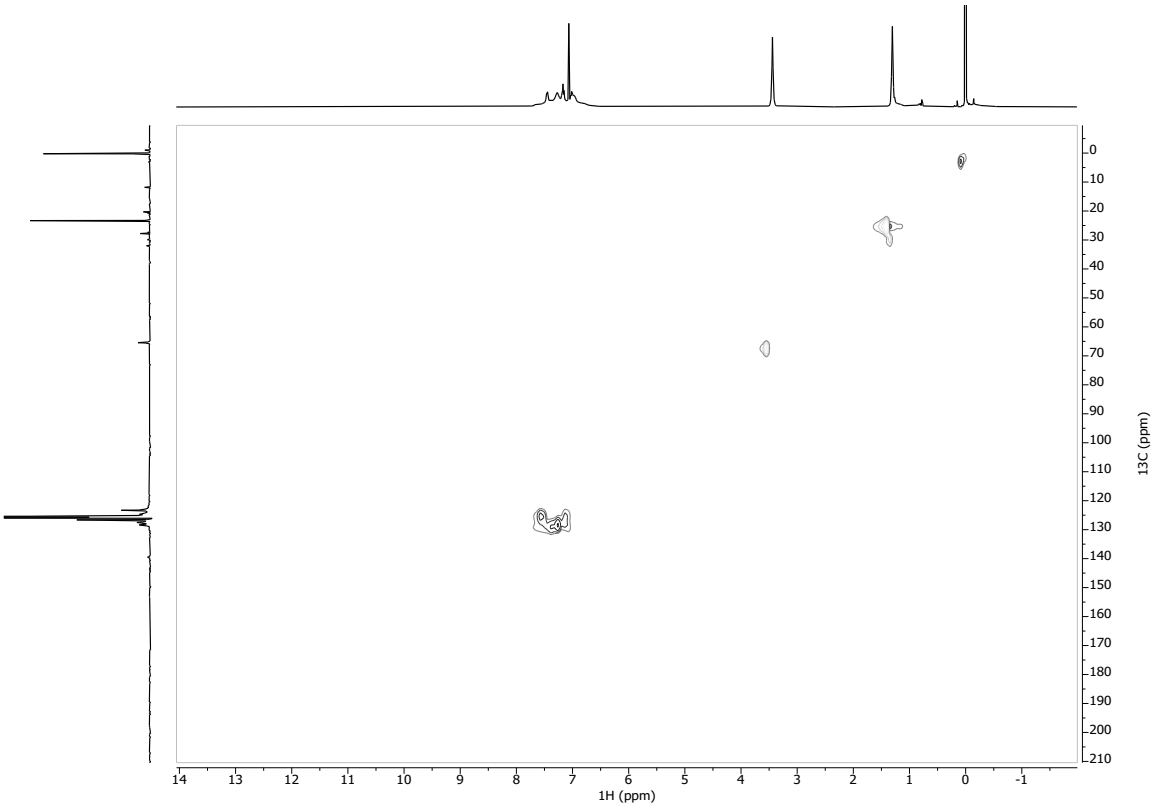

Figure S 16: HSQC-NMR-Spectrum (400 MHz, C_6D_6, 297 K) of $[(thf)_3Ba(NH\text{-}C_6H_2(Ph)_3)_2]$ **1e**.

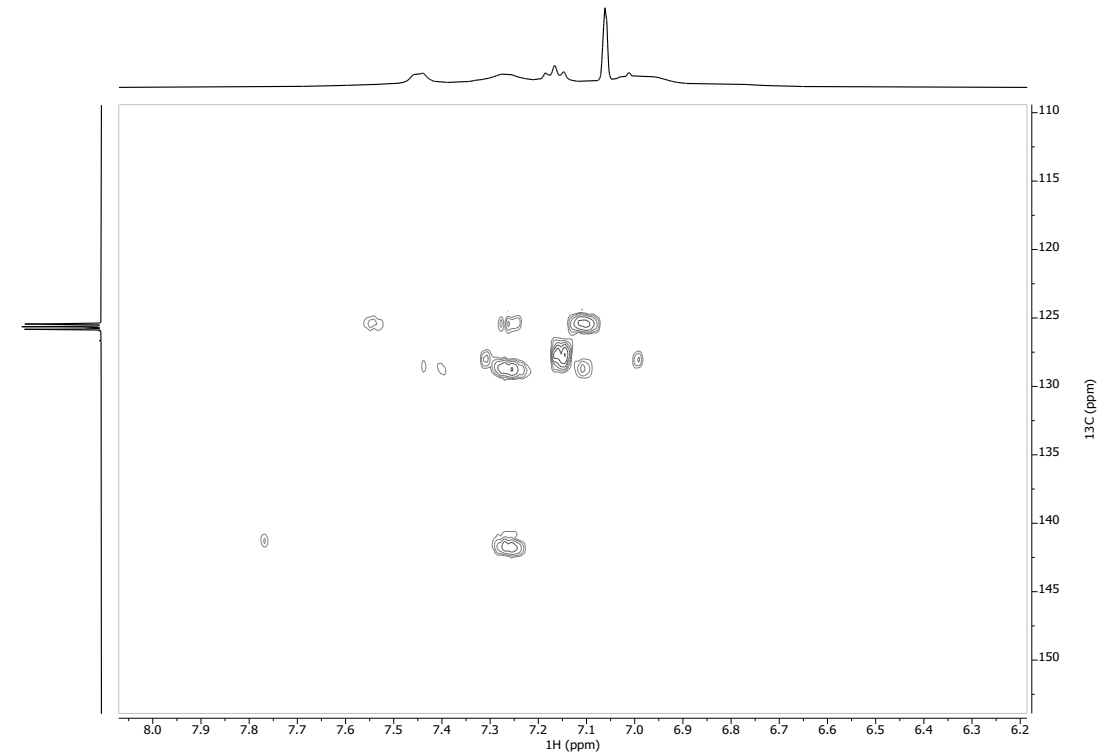

Figure S 17: HMBC-NMR-Spectrum (400 MHz, C_6D_6, 297 K) of $[(thf)_3Ba(NH\text{-}C_6H_2(Ph)_3)_2]$ **1e**.

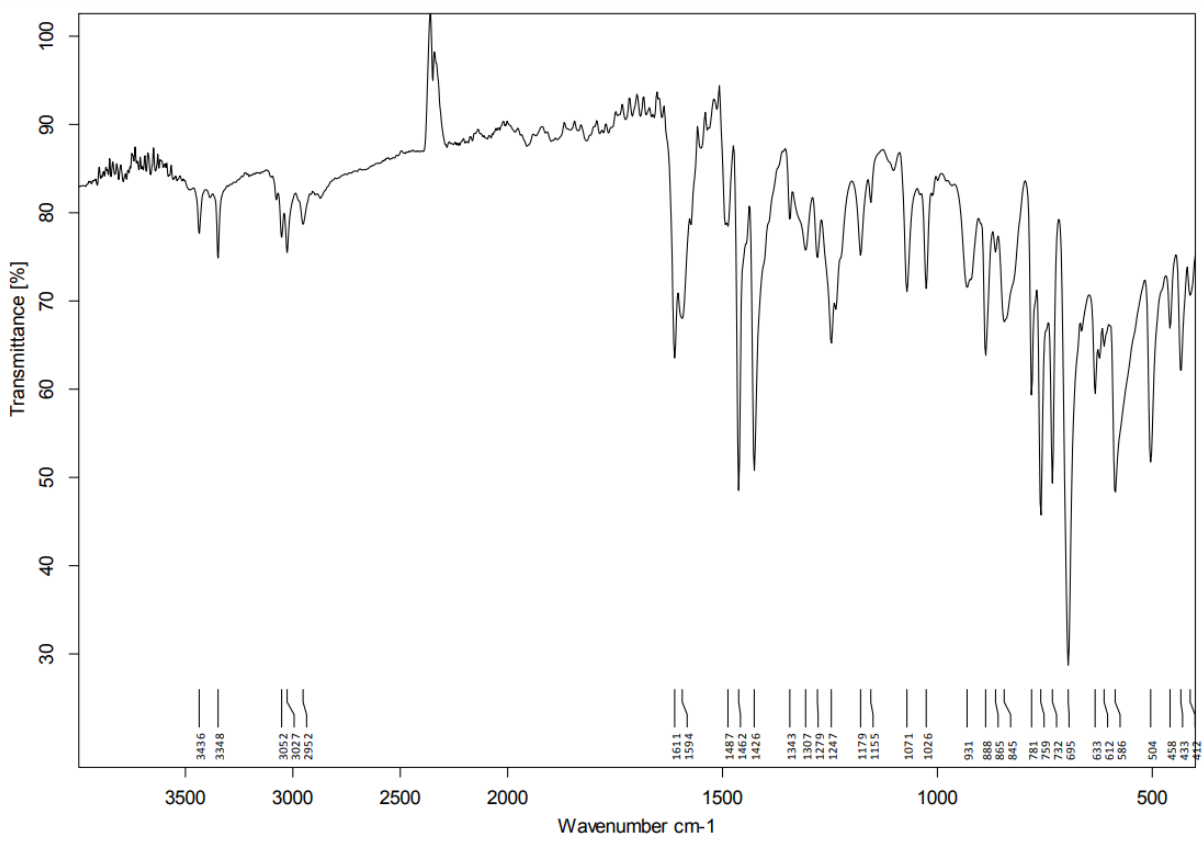

Figure S 18: IR spectrum (ATR) of $[(thf)_3Ba(NH\text{-}C_6H_2(Ph)_3)_2]$ **1e**.

1.5 $[(thf)_2Mg\{NH\text{-}2,6\text{-}(Ph_2CH)\text{-}4\text{-}Me\text{-}C_6H_2\}(^nBu/^sBu)]$ **2b$_{Bu}$**

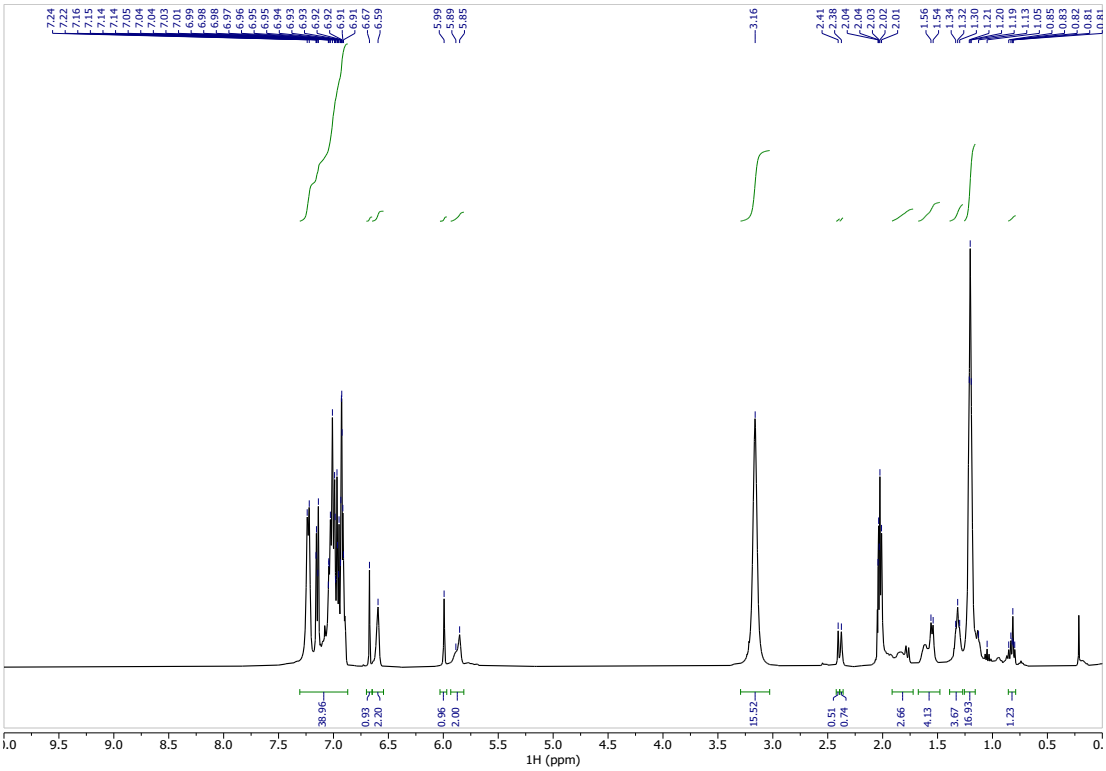

Figure S 19: ^{1}H-NMR-Spectrum (400 MHz, [D$_8$]Tol, 297 K) of $[(thf)_2Mg\{NH\text{-}2,6\text{-}(Ph_2CH)\text{-}4\text{-}Me\text{-}C_6H_2\}(^nBu/^sBu)]$ **2b$_{Bu}$**.

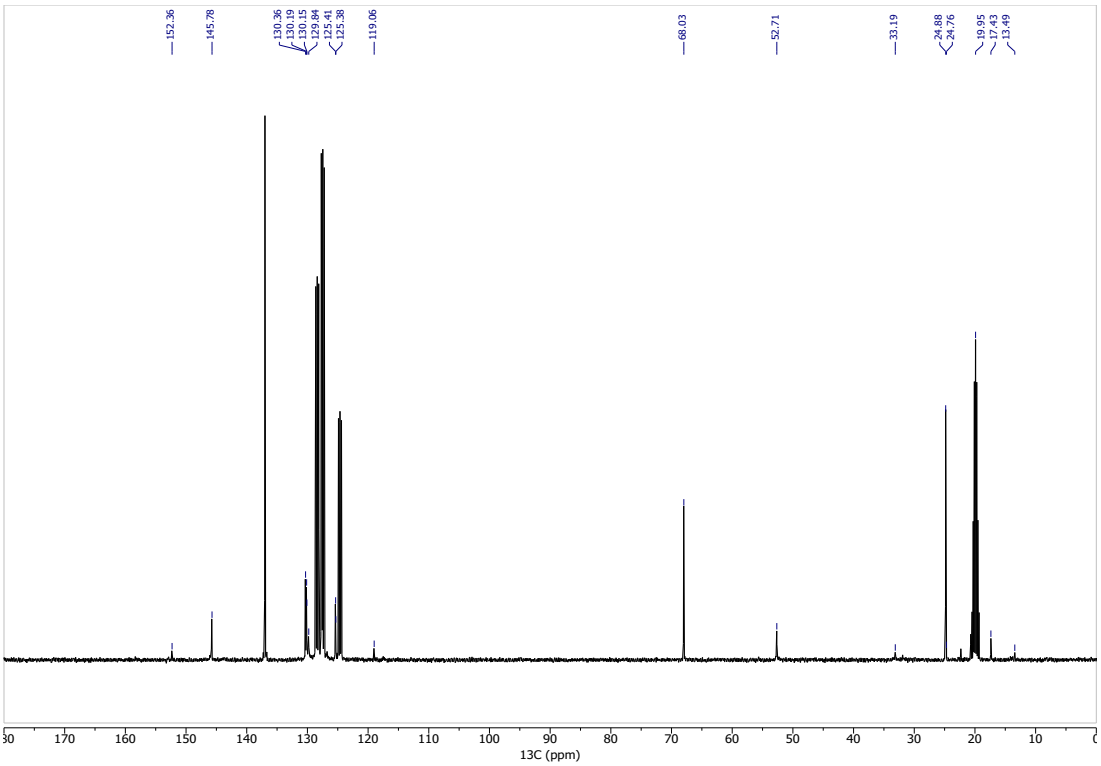

Figure S 20: $^{13}C\{^{1}H\}$-NMR-Spectrum (101 MHz, [D_8]Tol, 297 K) of [(thf)$_2$Mg {NH-2,6-(Ph_2CH)-4-Me-C_6H_2}(^{n}Bu/^{s}Bu)] **2b$_{Bu}$**.

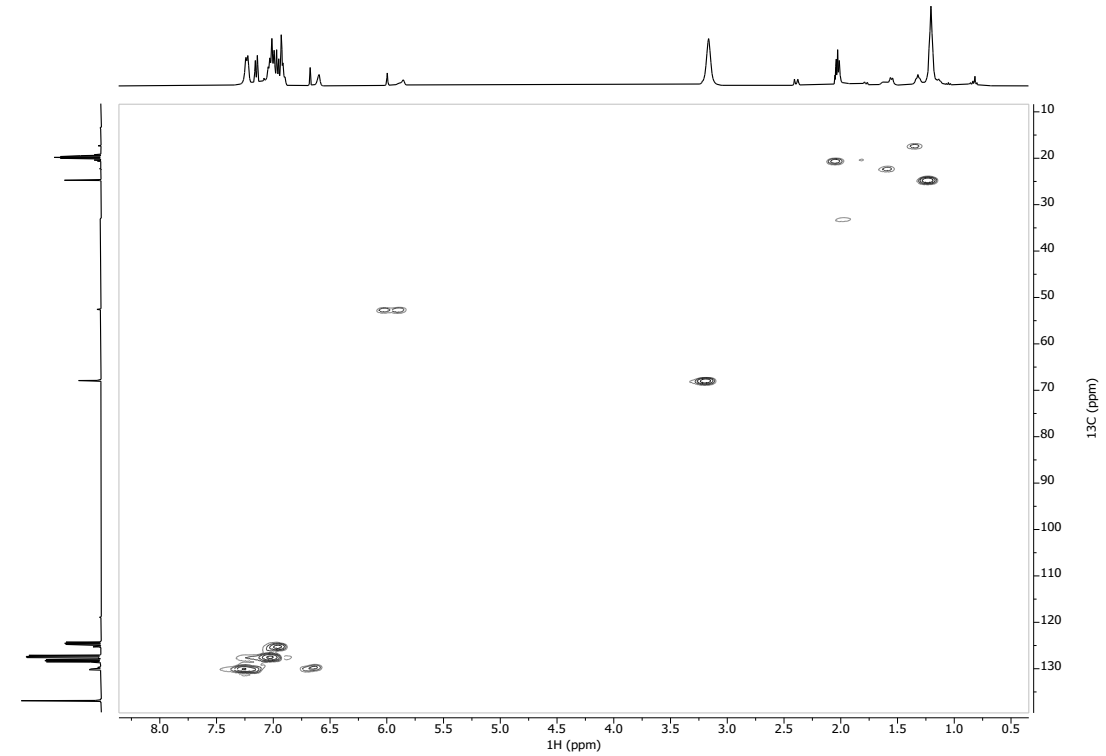

Figure S 21: HSQC-NMR-Spectrum (400 MHz, [D_8]Tol, 297 K) of [(thf)$_2$Mg {NH-2,6-(Ph_2CH)-4-Me-C_6H_2}(^{n}Bu/^{s}Bu)] **2b$_{Bu}$**.

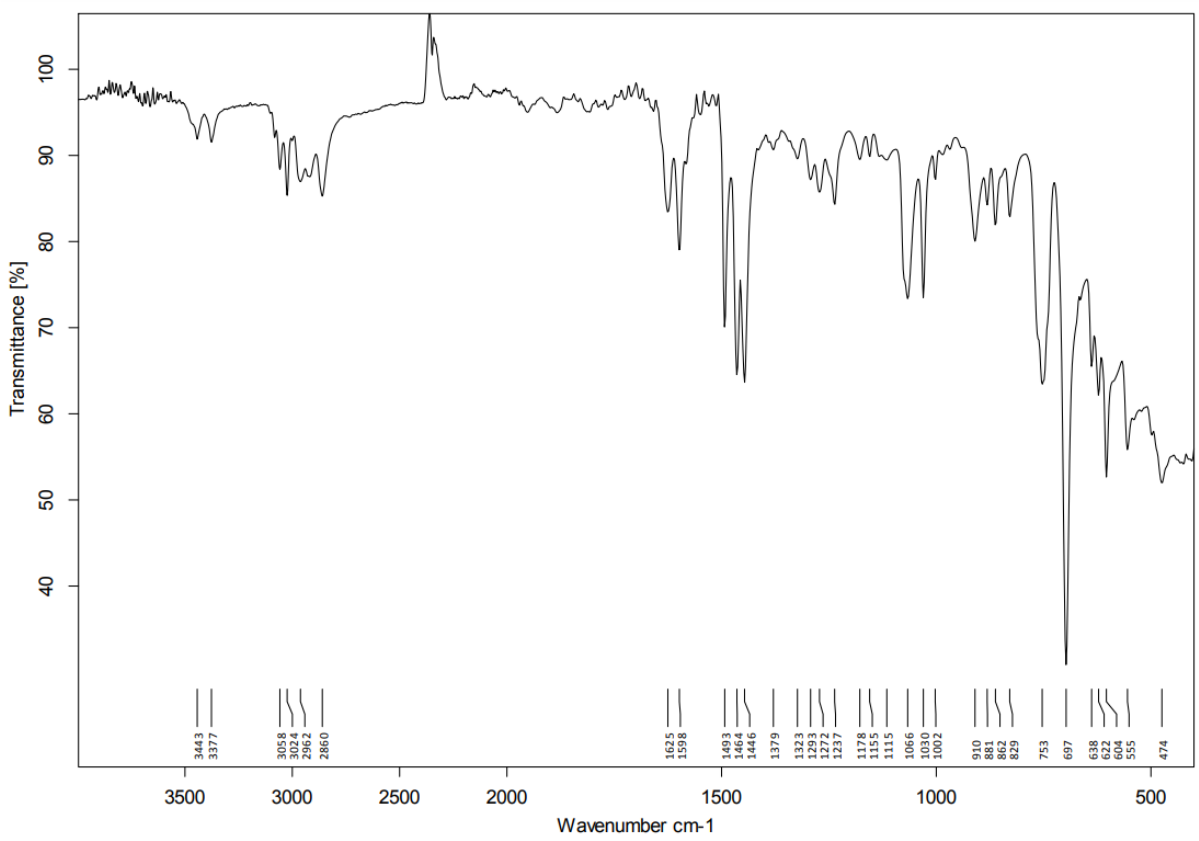

Figure S 22: IR spectrum of $[(thf)_2Mg\ \{NH\text{-}2,6\text{-}(Ph_2CH)\text{-}4\text{-}Me\text{-}C_6H_2\}(^nBu/^sBu)]$ **$2b_{Bu}$**.

1.6 $[(thf)_2Mg\{NH\text{-}2,6\text{-}(Ph_2CH)\text{-}4\text{-}Me\text{-}C_6H_2\}(Ph)]$ **2b$_{Ph}$**

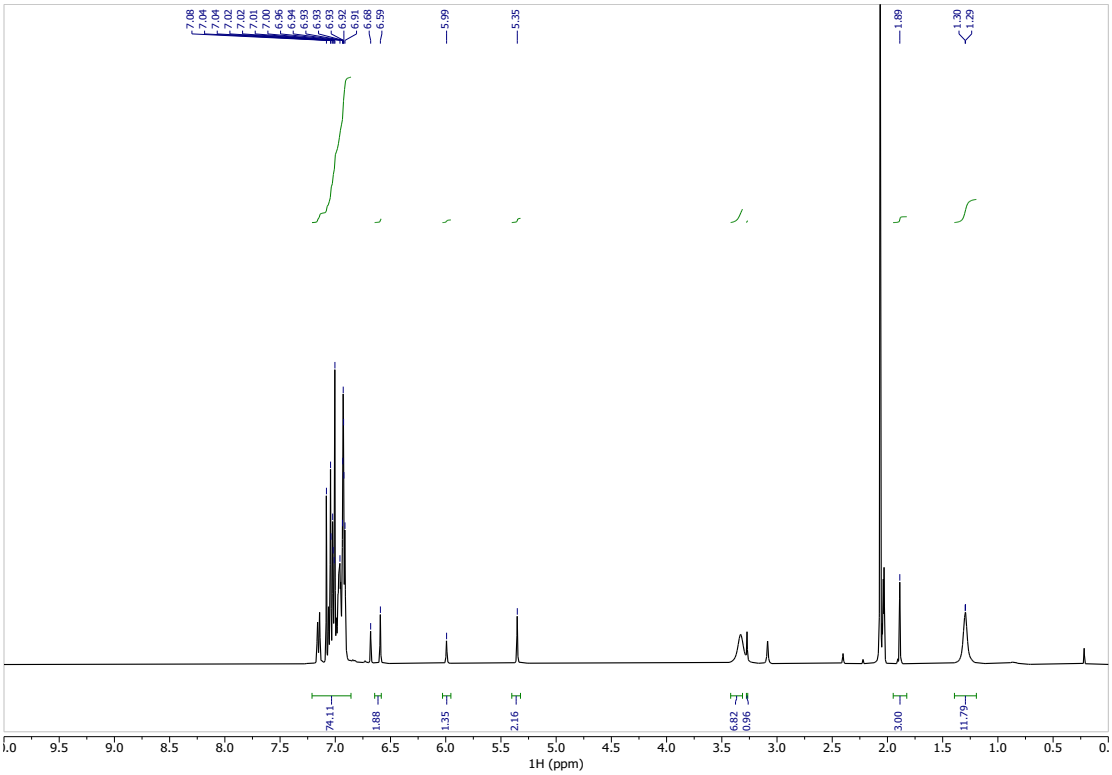

Figure S 23: ^{1}H-NMR-Spectrum (400 MHz, [D$_8$]Tol, 297 K) of $[(thf)_2Mg\{NH\text{-}2,6\text{-}(Ph_2CH)\text{-}4\text{-}Me\text{-}C_6H_2\}(Ph)]$ **2b$_{Ph}$**.

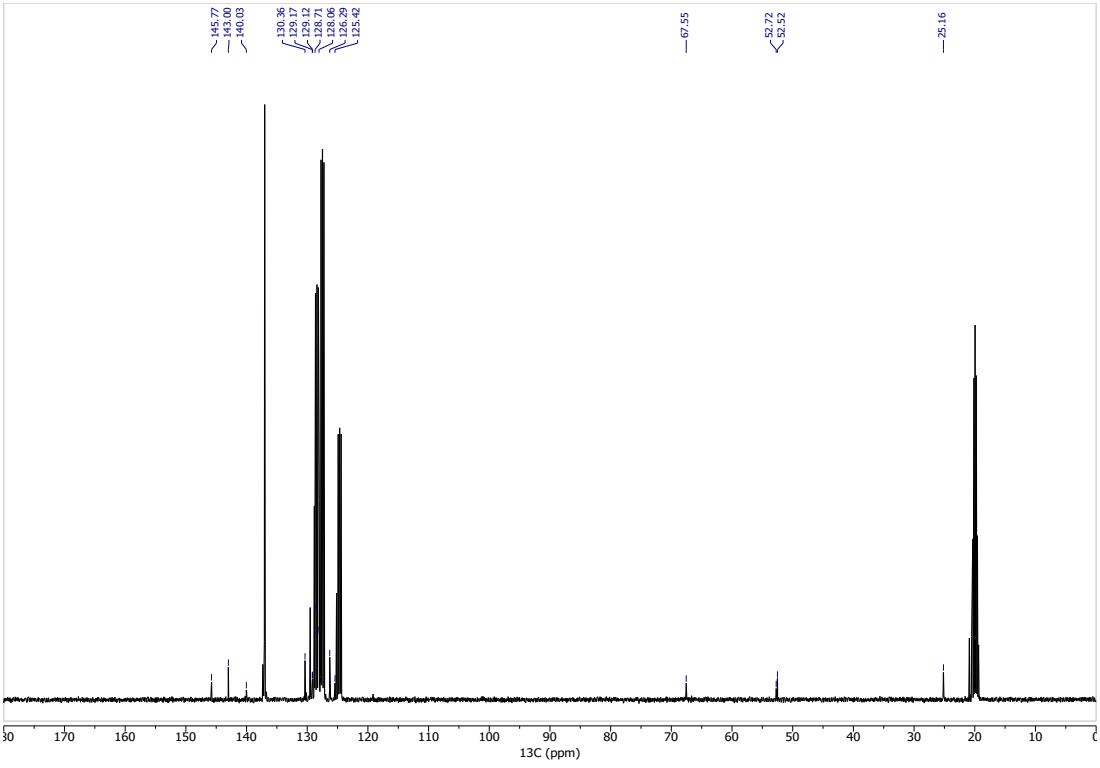

Figure S 24: $^{13}C\{^{1}H\}$-NMR-Spectrum (101 MHz, [D$_8$]Tol, 297 K) of $[(thf)_2Mg\{NH\text{-}2,6\text{-}(Ph_2CH)\text{-}4\text{-}Me\text{-}C_6H_2\}(Ph)]$ **2b$_{Ph}$**.

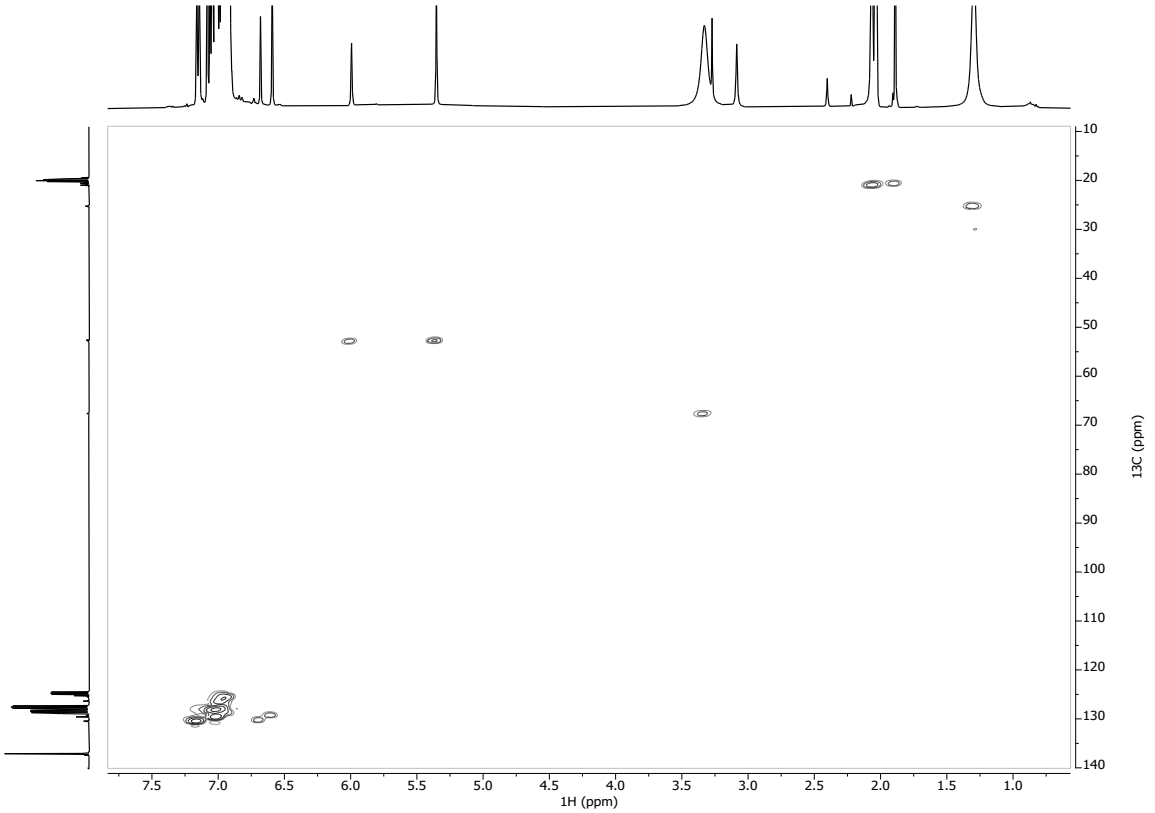

Figure S 25: HSQC-NMR-Spectrum (400 MHz, [D_8]Tol, 297 K) of [(thf)$_2$Mg {NH-2,6-(Ph_2CH)-4-Me-C_6H_2}(Ph)] **2b$_{Ph}$**.

1.7 $[(thf)_2Mg\{NH\text{-}2,6\text{-}(Ph_2CH)\text{-}4\text{-}Me\text{-}C_6H_2\}_2]$ **2b**

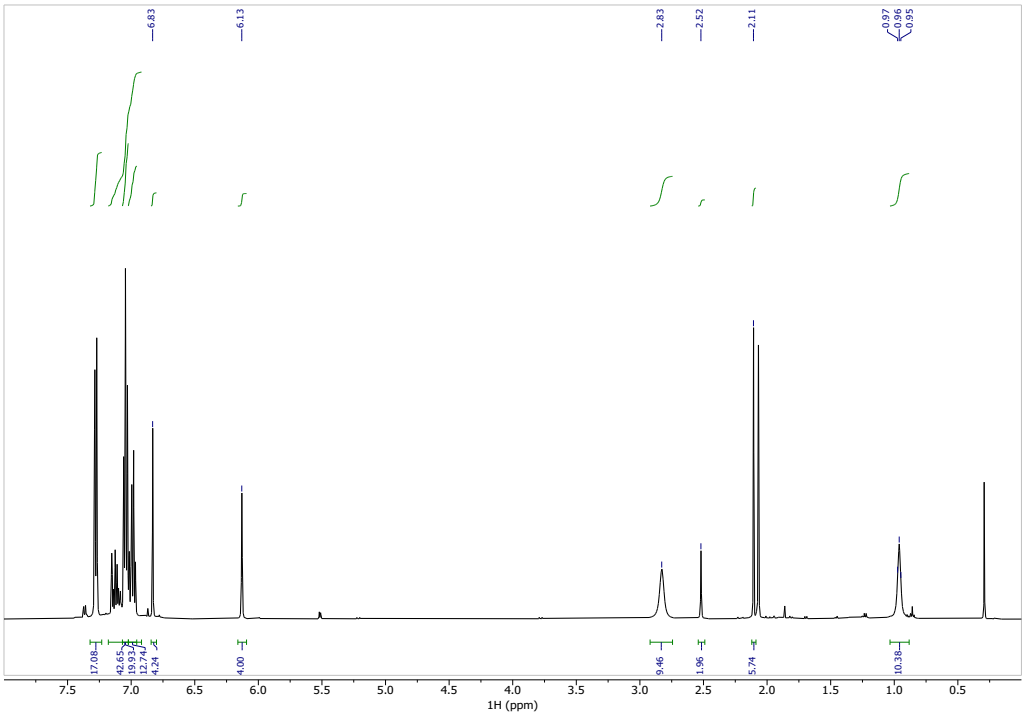

Figure S 26: ^{1}H-NMR-Spectrum (400 MHz, C_6D_6, 297 K) of $[(thf)_2Mg\{NH\text{-}2,6\text{-}(Ph_2CH)\text{-}4\text{-}Me\text{-}C_6H_2\}_2]$ **2b**. The sample contains substochiometric amounts of toluene.

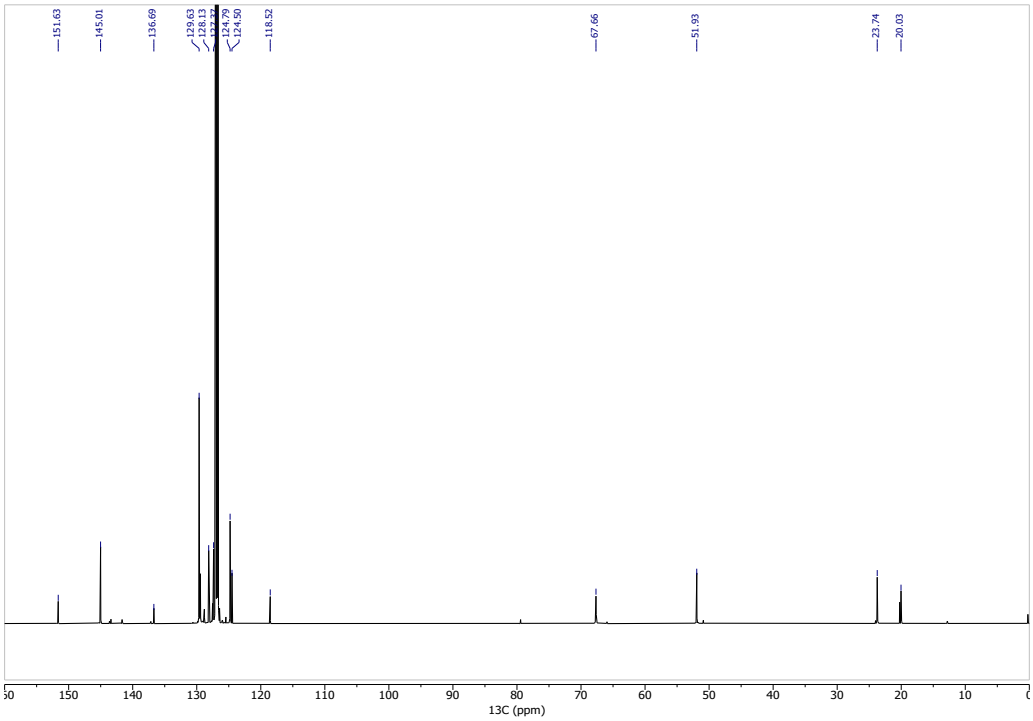

Figure S 27: $^{13}C\{^{1}H\}$-NMR-Spectrum (101 MHz, C_6D_6, 297 K) of $[(thf)_2Mg\{NH\text{-}2,6\text{-}(Ph_2CH)\text{-}4\text{-}Me\text{-}C_6H_2\}_2]$ **2b**. The sample contains substoichiometric amounts of toluene.

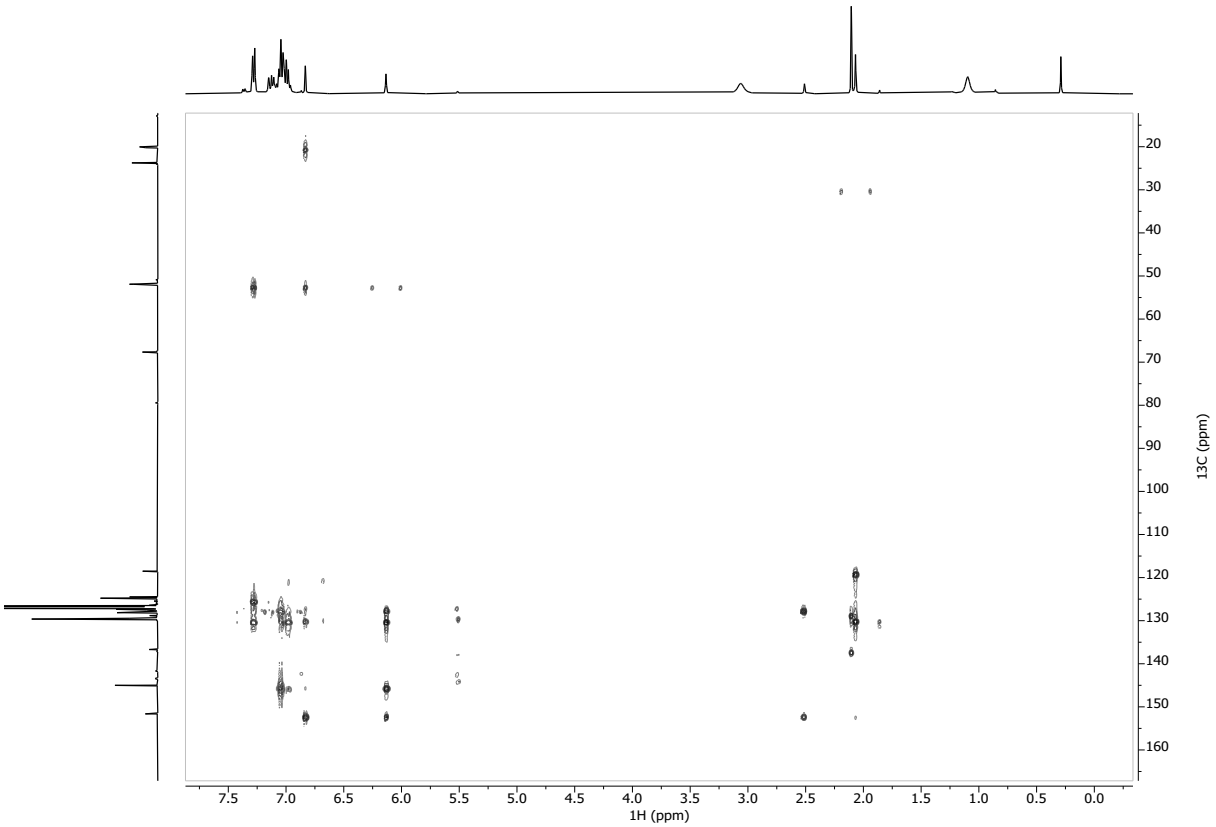

Figure S 28: HMBC-NMR-Spectrum (400 MHz, C_6D_6, 297 K) of [(thf)$_2$Mg {NH-2,6-(Ph_2CH)-4-Me-C_6H_2}$_2$] **2b**. The sample contains substochiometric amounts of toluene.

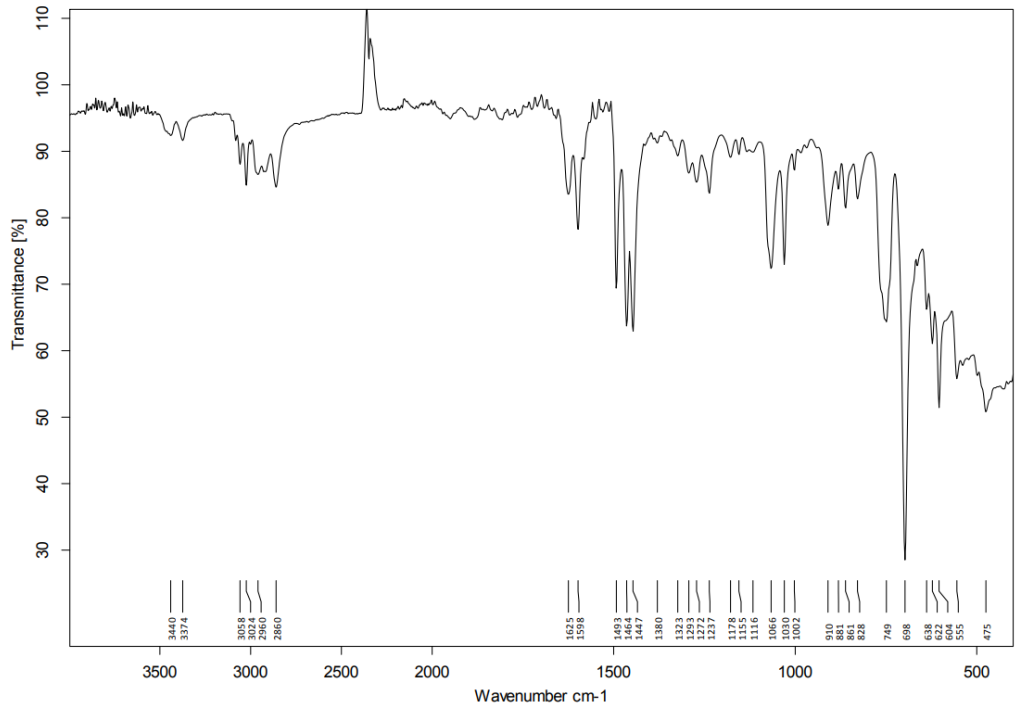

Figure S 29: IR spectrum of [(thf)$_2$Mg {NH-2,6-(Ph_2CH)-4-Me-C_6H_2}$_2$] **2b**.

1.8 $[(thf)_2Ca\{NH\text{-}2,6\text{-}(Ph_2CH)\text{-}4\text{-}Me\text{-}C_6H_2\}_2]$ **2c**

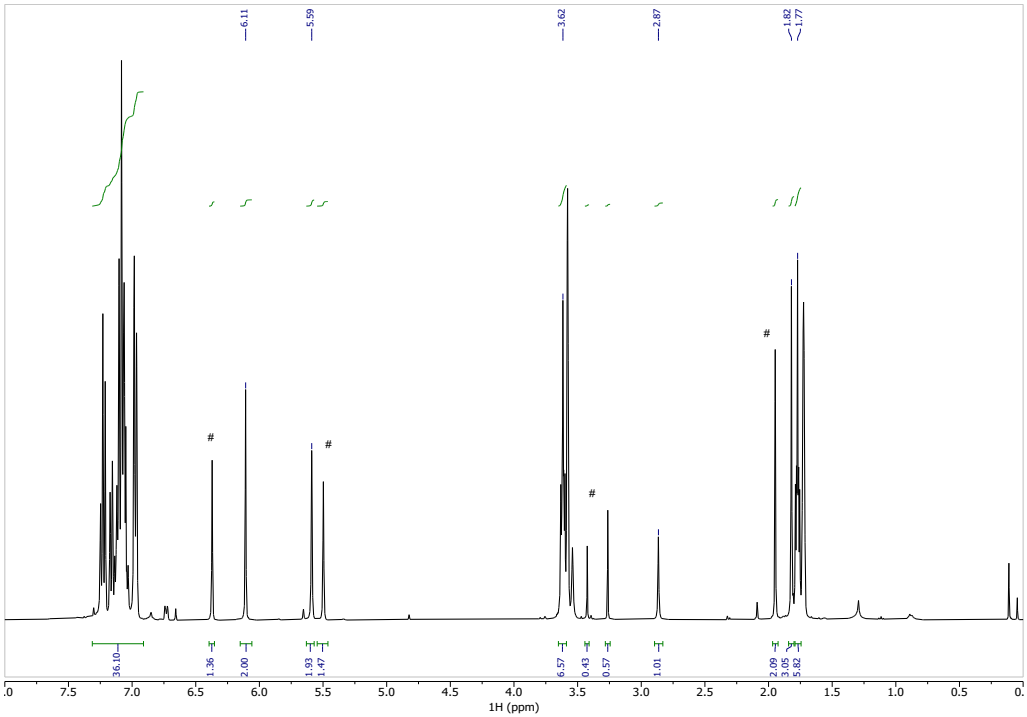

Figure S 30: ^{1}H-NMR-Spectrum (400 MHz, $[D_8]THF$, 297 K) of $[(thf)_2Ca\{NH\text{-}2,6\text{-}(Ph_2CH)\text{-}4\text{-}Me\text{-}C_6H_2\}_2]$ **2c**. The sample contains protonated aniline (#).

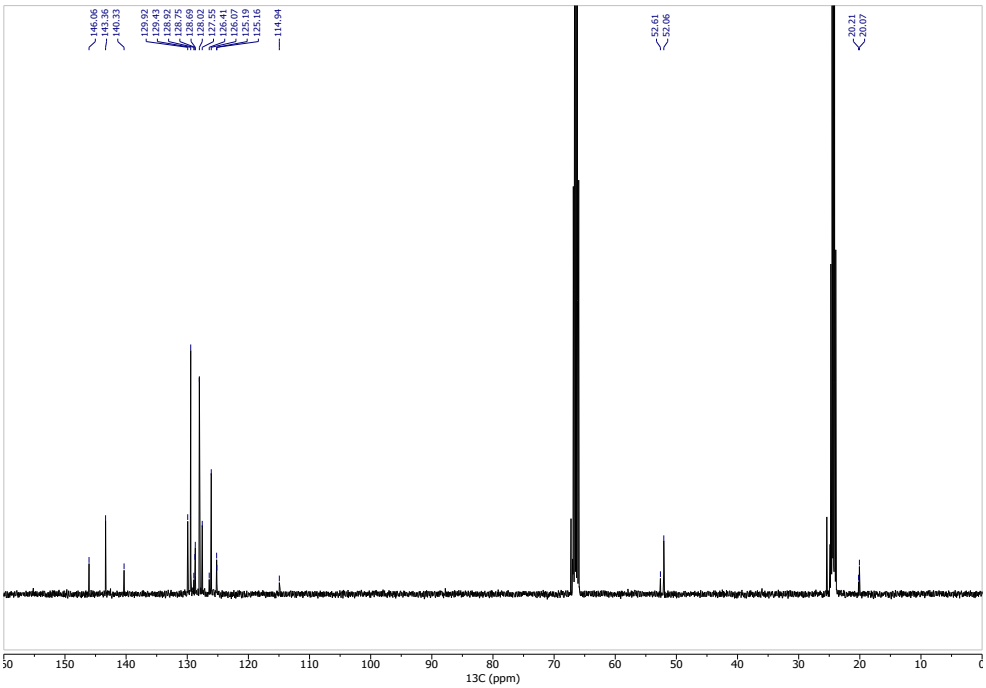

Figure S 31: $^{13}C\{^{1}H\}$-NMR-Spectrum (101 MHz, $[D_8]THF$, 297 K) of $[(thf)_2Ca\{NH\text{-}2,6\text{-}(Ph_2CH)\text{-}4\text{-}Me\text{-}C_6H_2\}_2]$ **2c**. The sample contains protonated aniline (#).

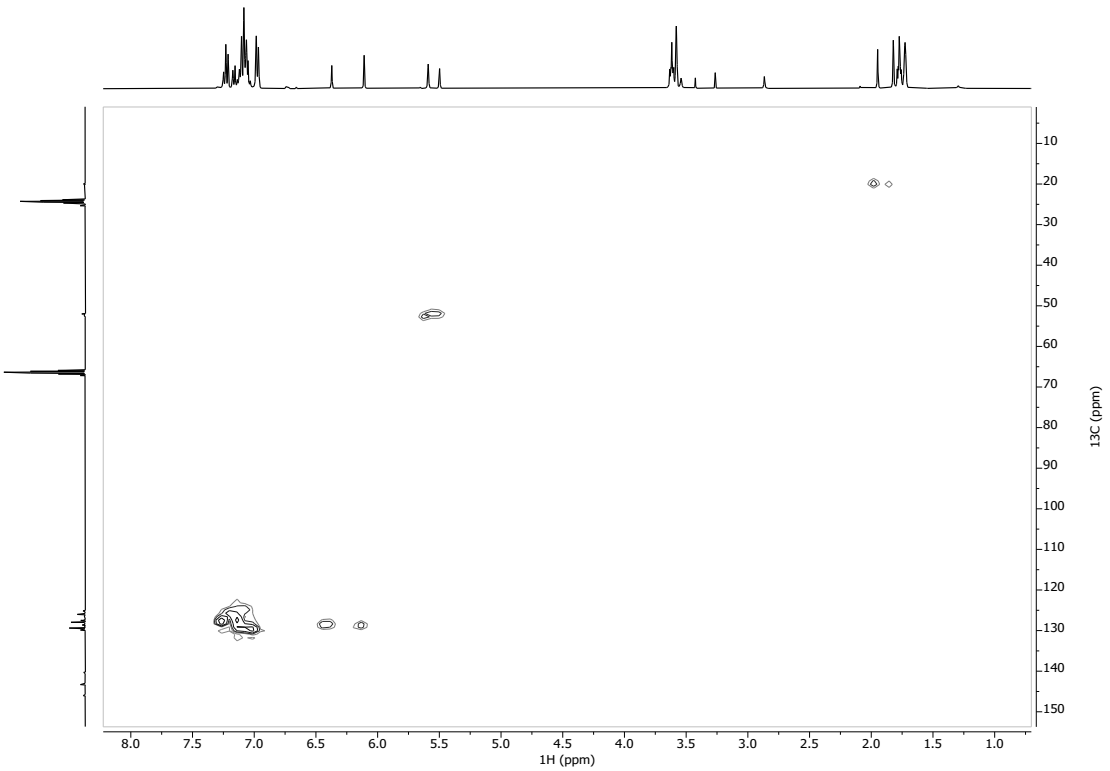

Figure S 32: HSQC-NMR-Spectrum (400 MHz, [D_8]THF, 297 K) of [(thf)$_2$Ca{NH-2,6-(Ph$_2$CH)-4-Me-C$_6$H$_2$}$_2$] **2c**. The sample contains protonated aniline (#).

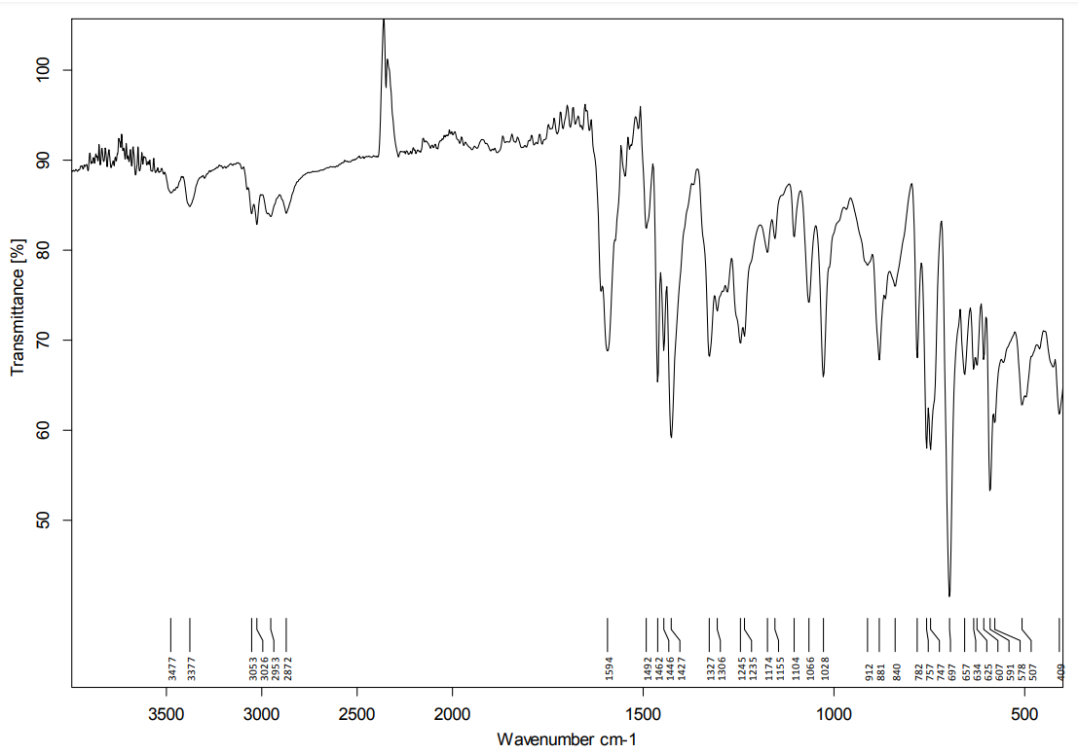

Figure S 33: IR spectrum (ATR) of [(thf)$_2$Ca{NH-2,6-(Ph$_2$CH)-4-Me-C$_6$H$_2$}$_2$] **2c**.

1.9 $[(thf)_2Sr\{NH\text{-}2\text{-}(Ph_2C)\text{-}6\text{-}(Ph_2CH)\text{-}4\text{-}Me\text{-}C_6H_2\}]_2$ **2d'**

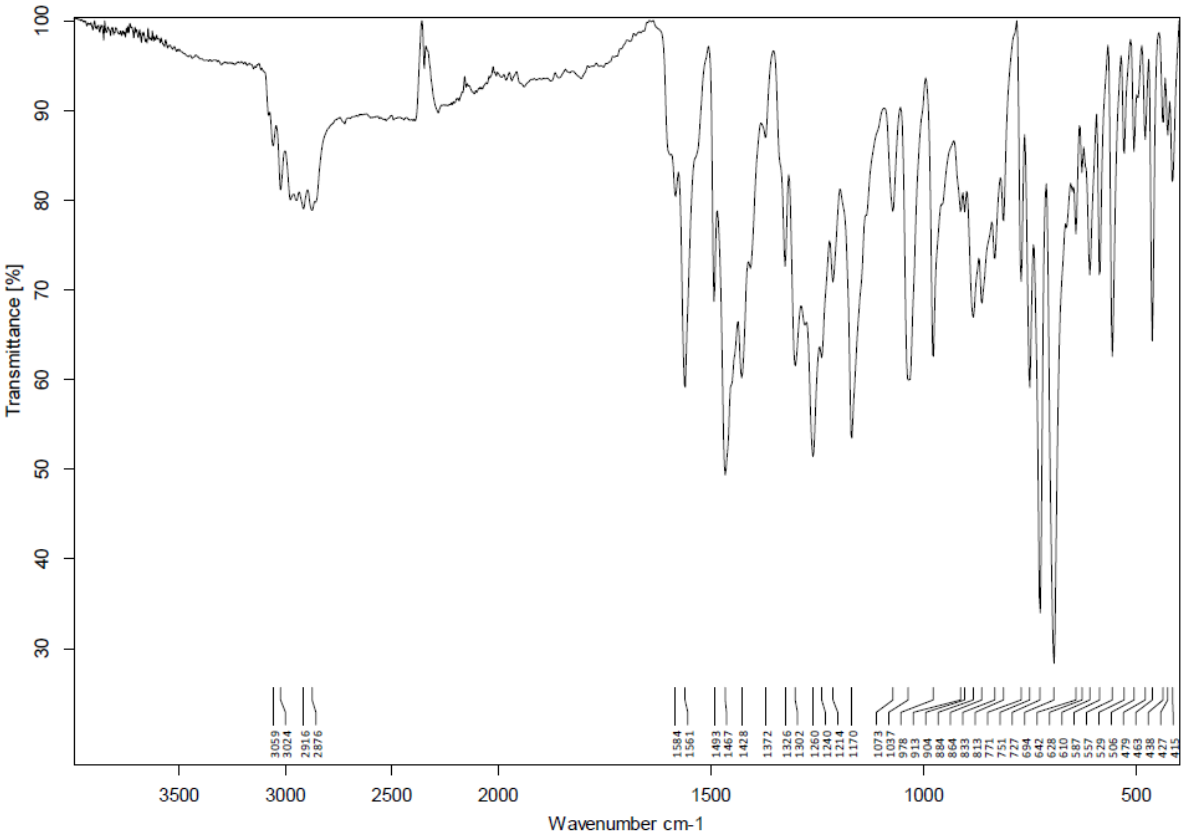

Figure S 34: IR spectrum (ATR) of [(thf)2Sr {NH-2-(Ph_2C)-6-(Ph_2CH)-4-Me-C_6H_2}]$_2$ **2d'**.

1.10 $[(thf)_2Sr\{NH\text{-}2,6\text{-}(Ph_2CH)_2\text{-}4\text{-}Me\text{-}C_6H_2\}_2]$ **2d**

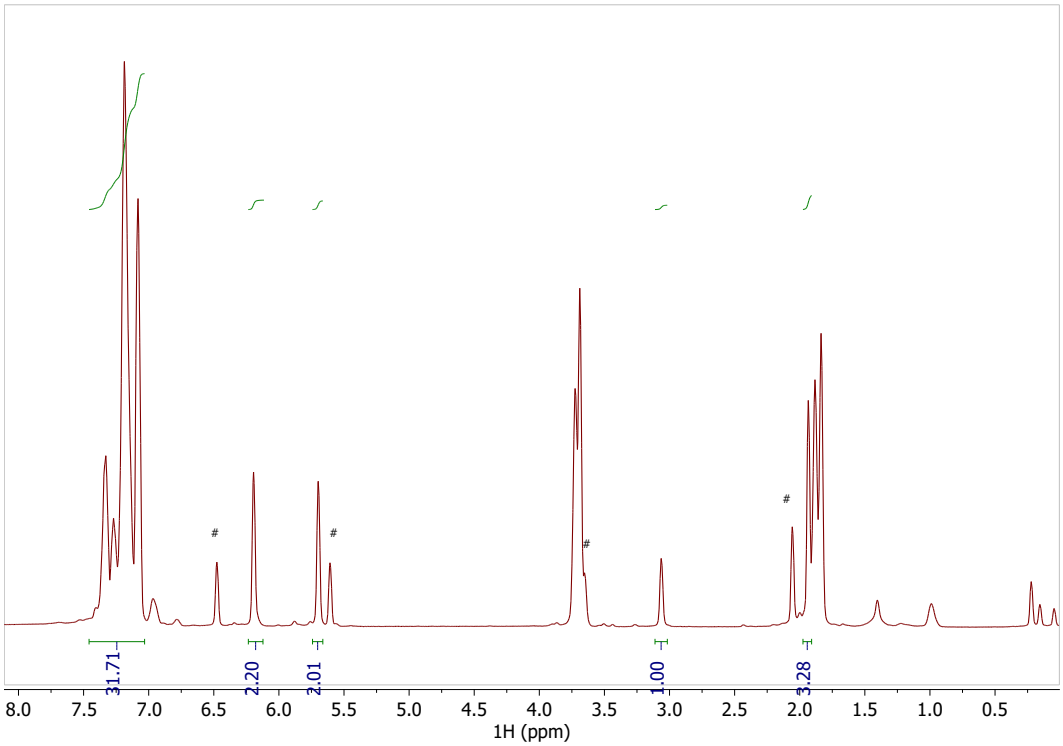

Figure S 35: ^{1}H-NMR spectrum ([D_8]THF, 297K, 400 MHz) of $[(thf)_2Sr\{NH\text{-}2,6\text{-}(Ph_2CH)_2\text{-}4\text{-}Me\text{-}C_6H_2\}_2]$ **2d**.

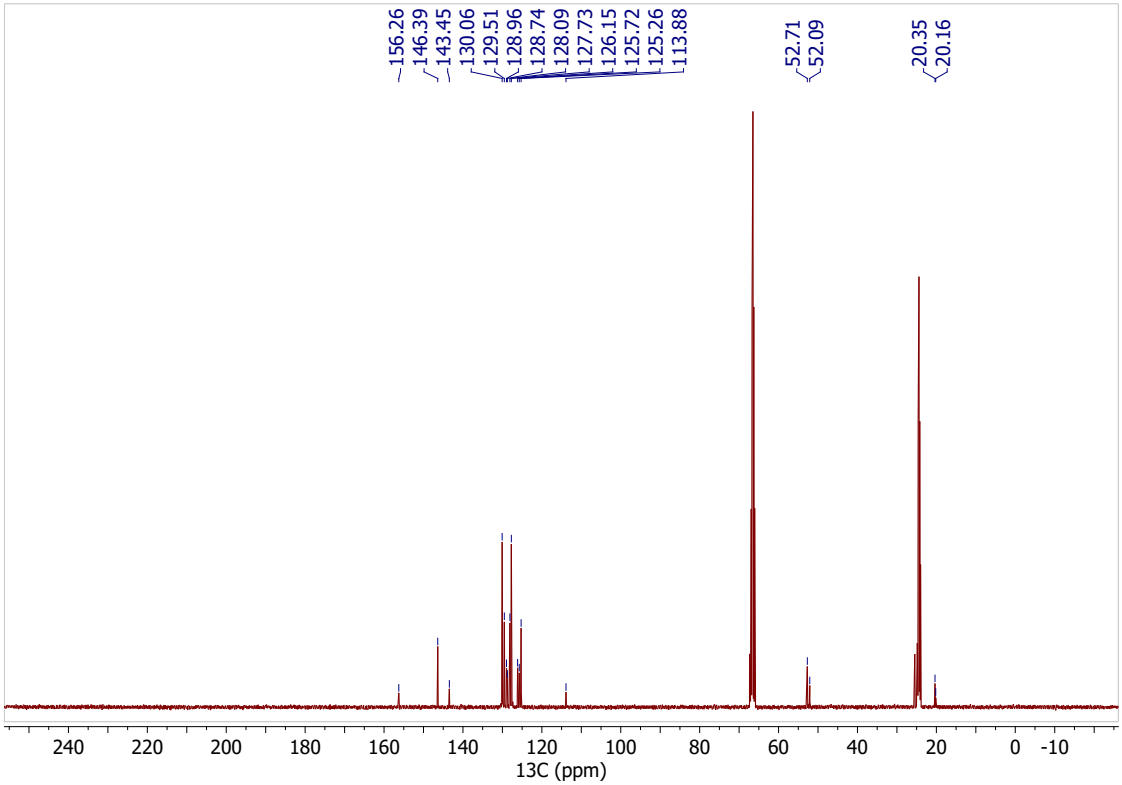

Figure S 36: $^{13}C\{^{1}H\}$-NMR spectrum ([D_8]THF, 297K, 101 MHz) of $[(thf)_2Sr\{NH\text{-}2,6\text{-}(Ph_2CH)_2\text{-}4\text{-}Me\text{-}C_6H_2\}_2]$ **2d**.

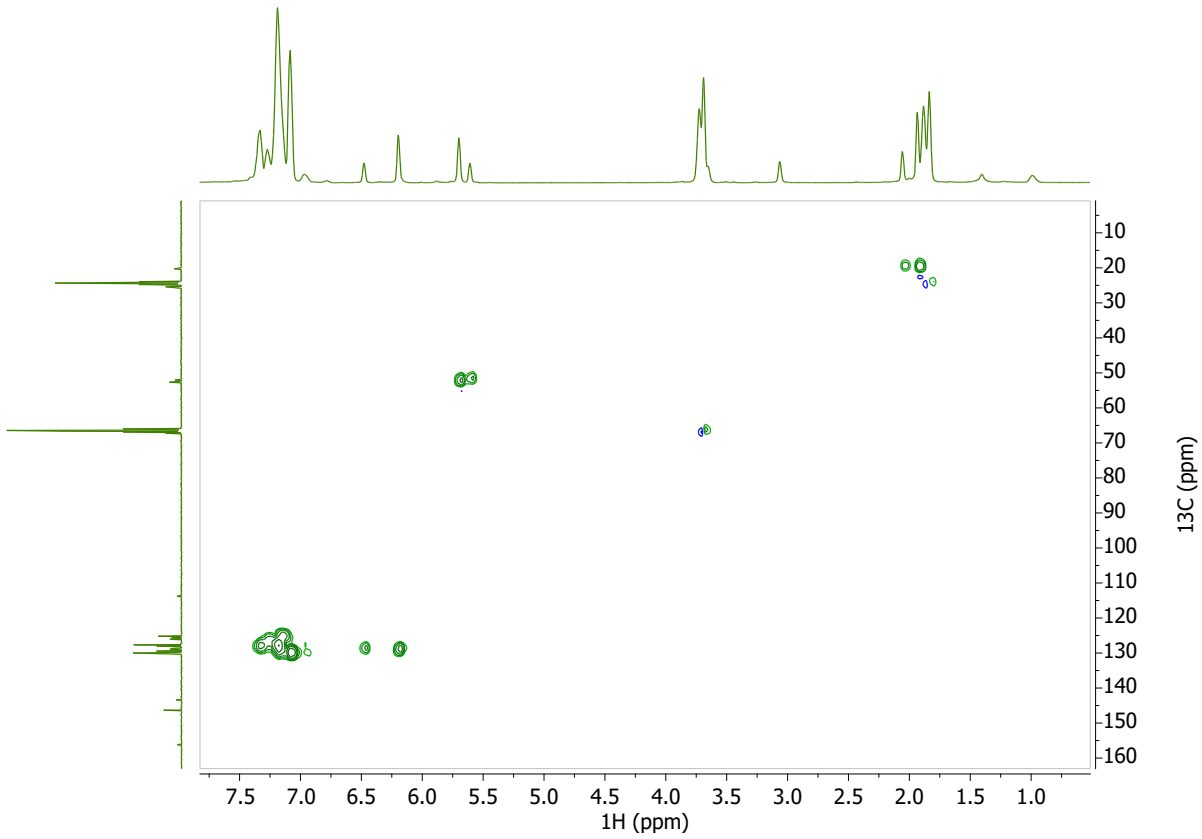

Figure S 37: HSQC-DEPT-NMR spectrum ([D_8]THF, 297K, 400 MHz) of [(thf)$_2$Sr{NH-2,6-(Ph_2CH)$_2$-4-Me-C_6H_2}$_2$] **2d**.

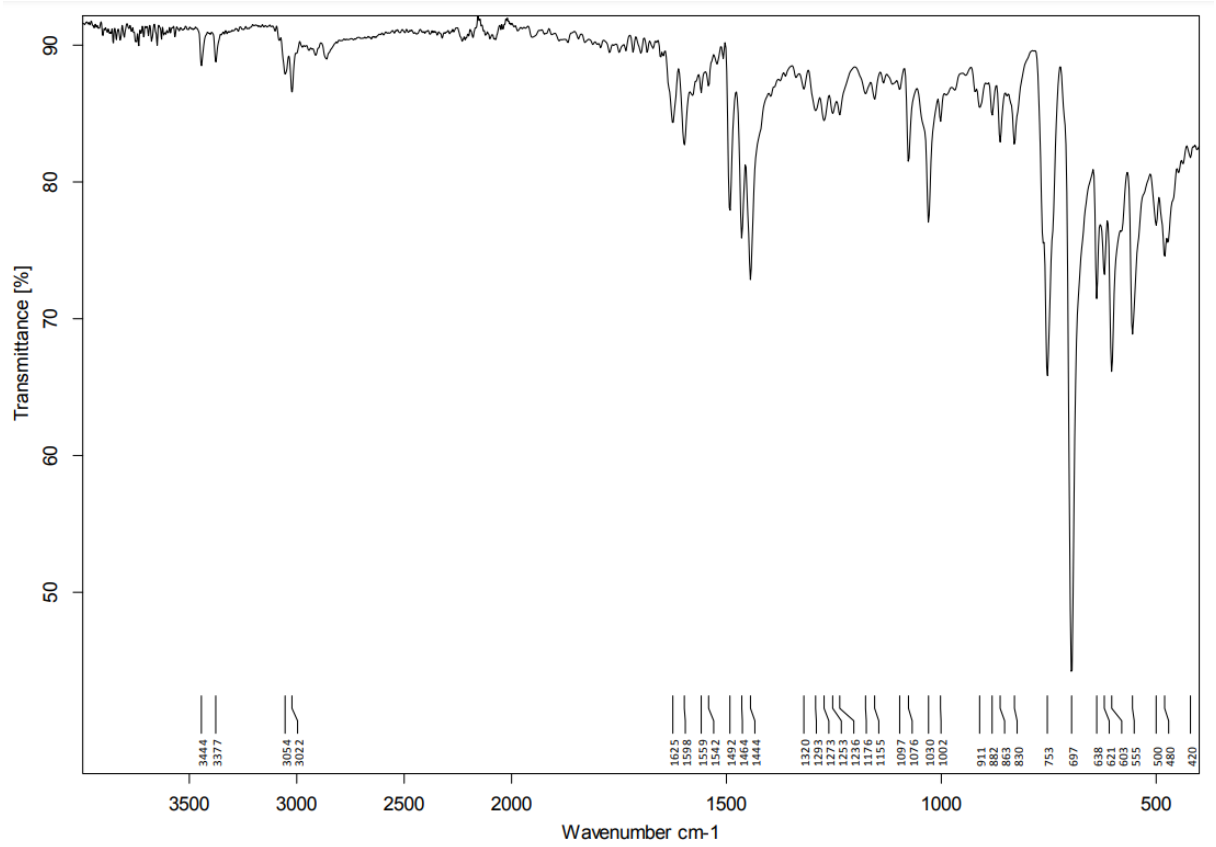

Figure S 38: IR spectrum (ATR) of $[(thf)_2Sr\{NH\text{-}2,6\text{-}(Ph_2CH)\text{-}4\text{-}Me\text{-}C_6H_2\}_2$ **2d**.

1.11 $[(thf)_2Ba\{NH\text{-}2\text{-}(Ph_2C)\text{-}6\text{-}(Ph_2CH)\text{-}4\text{-}Me\text{-}C_6H_2\}]_2$ **2e'**

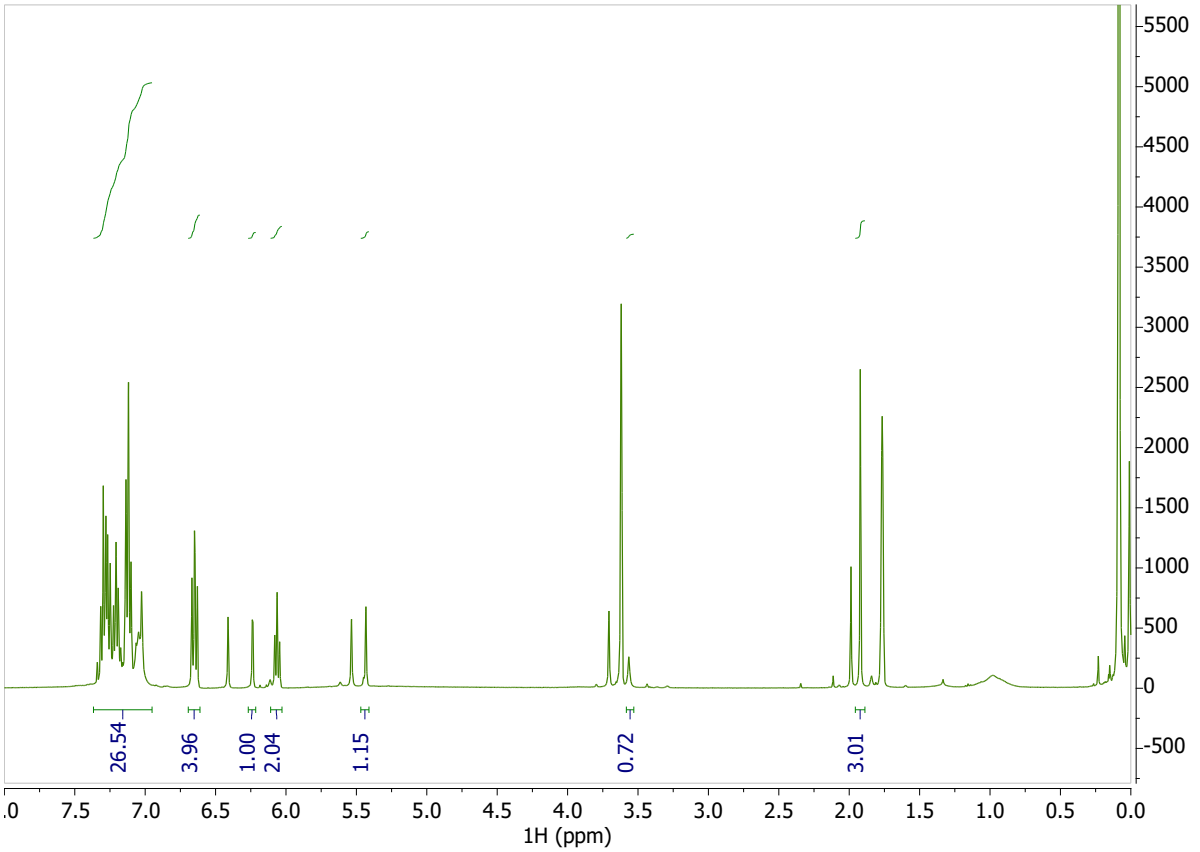

Figure S 39: ^{1}H-NMR-Spectrum (400 MHz, [D_8]THF, 297 K) of $[(thf)_2Ba\{NH\text{-}2\text{-}(Ph_2C)\text{-}6\text{-}(Ph_2CH)\text{-}4\text{-}Me\text{-}C_6H_2\}]$ **2e'**.

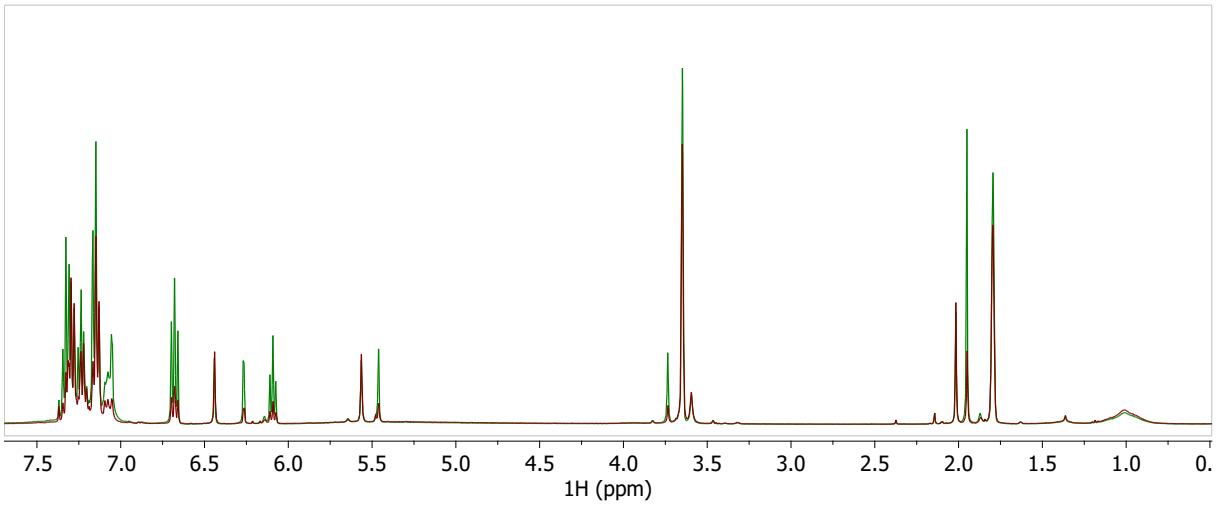

Figure S 40: Overlay of ^{1}H-NMR-Spectra (400 MHz, [D_8]THF, 297 K) *in situ* generated $[(thf)_2Ba\{NH\text{-}2\text{-}(Ph_2C)\text{-}6\text{-}(Ph_2CH)\text{-}4\text{-}Me\text{-}C_6H_2\}]$ **2e'** directly prepared (green) and after one hour (red). The compound **2e**' precipitated during this period in red crystals, yielding a intensity loss in ^{1}H-NMR spectrum.

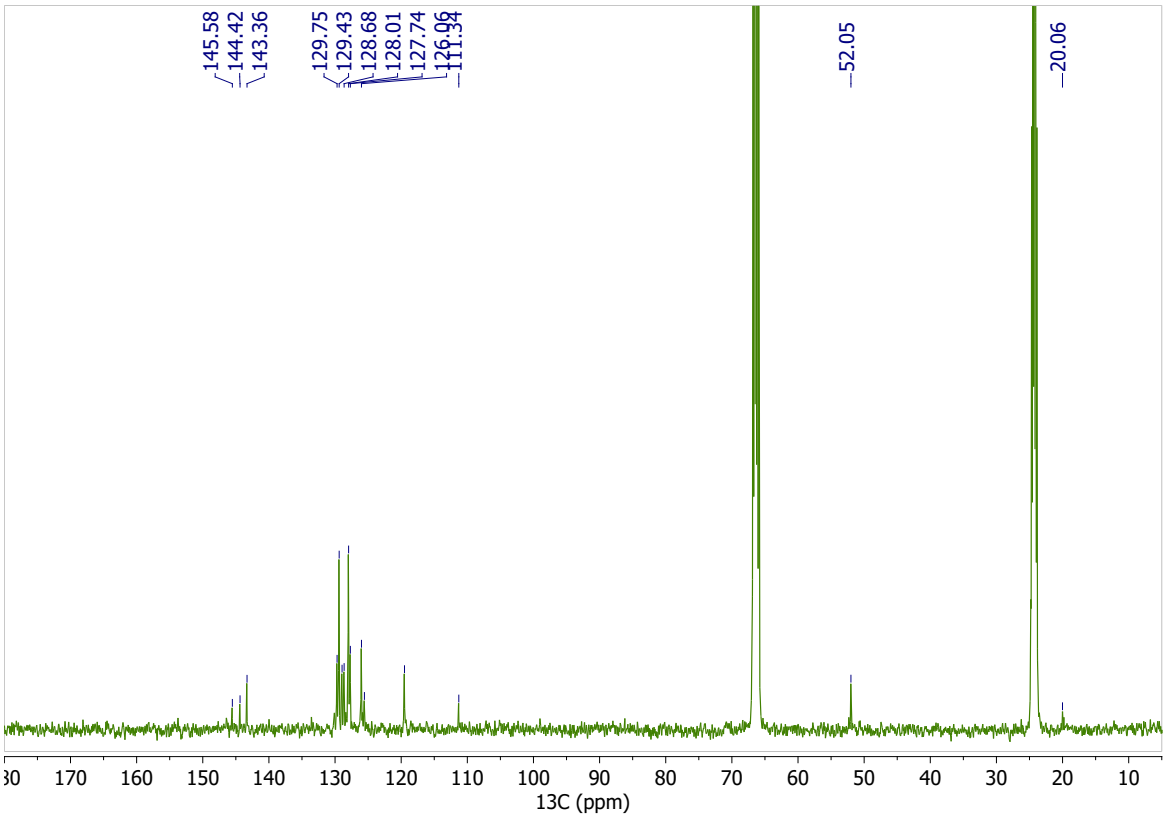

Figure S 41: $^{13}C\{^{1}H\}$-NMR-Spectrum (101 MHz, [D_8]THF, 297 K) of [(thf)$_2$Ba{NH-2-(Ph$_2$C)-6-(Ph$_2$CH)-4-Me-C$_6$H$_2$}] **2e'**.

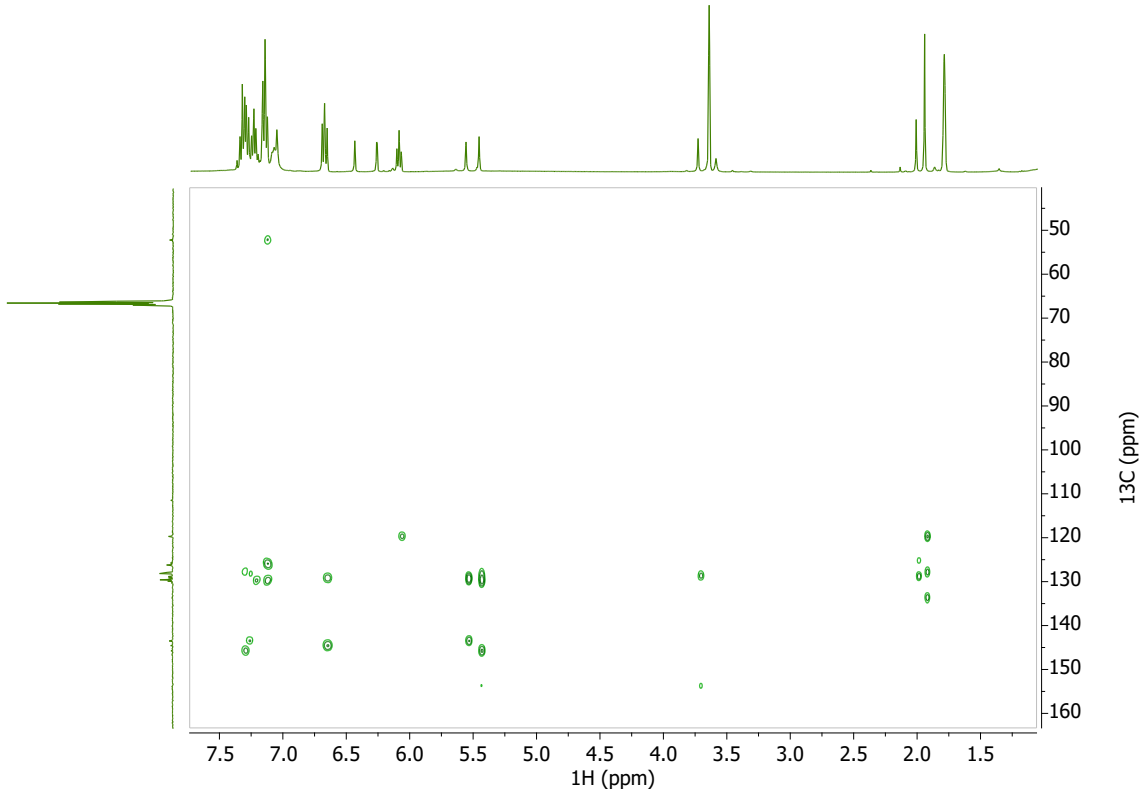

Figure S 42: ^{1}H-HMBC-NMR-Spectrum (400 MHz, [D_8]THF, 297 K) of [(thf)$_2$Ba{NH-2-(Ph$_2$C)-6-(Ph$_2$CH)-4-Me-C$_6$H$_2$}] **2e'**.

2 Crystallographic data

Table S 1: Crystal data and refinement details for the X-ray structure determinations.

Compound	**1b**	**1c**	**1d**	**2b$_{Bu}$**	**2b$_{Ph}$**
formula	$C_{60}H_{60}MgN_2O_3$	$C_{56}H_{52}CaN_2O_2$	$C_{60}H_{60}N_2O_3Sr$[*]	$C_{45}H_{53}MgNO_2$	$C_{47}H_{49}MgNO_2$
fw (g·mol^{-1})	881.41	825.07	944.72[*]	664.19	684.18
T/°C	-140(2)	-140(2)	-140(2)	-140(2)	-140(2)
crystal system	monoclinic	triclinic	Triclinic	monoclinic	monoclinic
space group	P 2_1/c	P $\bar{1}$	P $\bar{1}$	C 2/c	C 2/c
a/ Å	21.6285(5)	9.7673(3)	11.8826(2)	27.9665(5)	28.1647(5)
b/ Å	10.8549(2)	11.2864(4)	20.3808(4)	17.3376(4)	17.8406(4)
c/ Å	21.1559(4)	11.3300(3)	23.1208(4)	18.9540(5)	18.1355(3)
α/°	90	62.604(2)	66.247(1)	90	90
β/°	103.708(1)	82.371(2)	78.218(1)	124.620(1)	124.063(1)
γ/°	90	86.915(1)	84.243(1)	90	90
V/Å^3	4825.40(17)	1099.06(6)	5016.01(16)	7563.0(3)	7549.1(3)
Z	4	1	4	8	8
ρ (g·cm^{-3})	1.213	1.247	1.251[*]	1.167	1.204
μ (cm^{-1})	0.85	1.88	11.22[*]	0 .85	0.87
measured data	28122	13616	59383	40739	21851
data with $I > 2\sigma(I)$	8168	3995	16074	6309	6510
unique data (R_{int})	10982/0.0562	4987/0.0448	22603/0.0441	8671/0.0497	8616/0.0480
wR_2 (all data, on F^2)[a)]	0.1505	0.1617	0.2358	0.2154	0.1400
R_1 ($I > 2\sigma(I)$) [a)]	0.0667	0.0698	0.0902	0.0884	0.0651
s [b)]	1.075	1.055	1.087	1.079	1.089
Res. dens./e·Å^{-3}	0.366/-0.336	0.381/-0.589	2.276/-1.086	1.362/-0.406	0.658/-0.333
absorpt method	multi-scan	multi-scan	multi-scan	multi-scan	multi-scan
absorpt corr $T_{min/max}$	0.6592/0.7456	0.6891/0.7456	0.6564/0.7456	0.6796/0.7456	0.6895/0.7456
CCDC No.	2152421	2152422	2152423	2152424	2152425

Contd. Table S 1: Crystal data and refinement details for the X-ray structure determinations.

Compound	**2b**	**2c**	**2d**	**2d'**	**2e'**
formula	$C_{78}H_{80}MgN_2O_3$	$C_{86}H_{96}CaN_2O_5$	$C_{74}H_{72}N_2O_2Sr$	$C_{82}H_{86}N_2O_4Sr_2$[*]	$C_{96}H_{102}Ba_2N_2O_4$
fw ($g \cdot mol^{-1}$)	1117.75	1277.72	1108.95	1338.76[*]	1622.47
°*C*	-140(2)	-140(2)	-153(2)	-140(2)	-140(2)
crystal system	triclinic	orthorhombic	triclinic	triclinic	triclinic
space group	P $\bar{1}$	F d d 2	P $\bar{1}$	P $\bar{1}$	P $\bar{1}$
a/ Å	11.6149(2)	30.1857(5)	9.7312(13)	11.4529(4)	11.4133(3)
b/ Å	11.8127(3)	34.5680(5)	12.4502(15)	12.3964(3)	12.6652(3)
c/ Å	23.2496(5)	13.7013(2)	13.6436(17)	14.2573(4)	14.4790(3)
α/°	103.213(1)	90	99.627(5)	76.074(2)	73.278(1)
β/°	95.942(1)	90	108.743(6)	83.267(1)	82.423(1)
γ/°	93.433(1)	90	104.168(6)	82.325(2)	81.815(1)
V/Å^3	3077.27(12)	14296.7(4)	1462.3(3)	1939.45(10)	1974.90(8)
Z	2	8	1	1	1
ρ ($g \cdot cm^{-3}$)	1.206	1.187	1.259	1.146[*]	1.364
μ (cm^{-1})	.81	1.42	9.71	14.21[*]	10.45
measured data	33576	45739	18360	23046	10609
data with $I > 2\sigma(I)$	9907	7433	5799	6848	7893
unique data (R_{int})	12477/0.0484	8180/0.0473	7228/0.0437	8773/0.0492	8414/0.0252
wR_2 (all data, on F^2)[a)]	0.2582	0.0897	0.1003	0.1410	0.1005
R_1 ($I > 2\sigma(I)$) [a)]	0.0956	0.0454	0.0454	0.0696	0.0454
s [b)]	1.087	1.078	1.029	1.033	1.083
Res. dens./$e \cdot Å^{-3}$	0.703/-0.432	0.223/-0.218	0.432/-0.463	1.770/-0.447	1.208/-0.674
Flack-parameter	-	0.17(4)	-	-	-
absorpt method	multi-scan	multi-scan	multi-scan	multi-scan	multi-scan
absorpt corr $T_{min/max}$	0.6305/0.7456	0.6954/0.7391	0.6193/0.7456	0.6625/0.7456	0.6719/0.7456
CCDC No.	2152426	2152427	2161838	2152428	2152429

[*] derived parameters do not contain the contribution of the disordered solvent.

[a)] Definition of the *R* indices: $R_1 = (\Sigma \,||F_o| - |F_c||)/\Sigma|F_o|$;

$wR_2 = \{\Sigma[w(F_o^2-F_c^2)^2]/\Sigma[w(F_o^2)^2]\}^{1/2}$ with $w^{-1} = \sigma^2(F_o^2) + (aP)^2+bP$; $P = [2F_c^2 + \mathrm{Max}(F_o^2]/3$; [b)] $s = \{\Sigma[w(F_o^2-F_c^2)^2]/(N_o-N_p)\}^{1/2}$.